Sediment Composition in the Gulf of Cádiz Contourites during the Pleistocene

Research Thesis

Presented in partial fulfillment of the requirements for graduation
with research distinction in Geological Sciences in the undergraduate
colleges of The Ohio State University

by

Erin Lathrop
The Ohio State University
May 2015

Project Advisor: Dr. Lawrence Krissek, School of Earth Sciences

TABLE OF CONTENTS

ABSTRACT

The Gulf of Cádiz and West Iberian margin are the location of a complex contourite depositional system. Expedition 339 of the Integrated Ocean Drilling Program collected sediment cores from multiple sites in this area. In order to understand the history of the Mediterranean Outflow Water and how it has changed through glacial and interglacial periods, primary mineral phases in samples from two sites were identified. X-Ray diffraction (XRD) analyses of randomly oriented pressed powders were used to determine bulk mineralogy. Diffraction peak intensity ratios of major mineral phases, relative to quartz, provide a semiquantitative analysis. Ages were calculated using the shipboard age/depth model based on paleomagnetic and biostratigraphic data, and range from 300 ka to 1 Ma, covering multiple glacial cycles.

Fifty-four samples were used from Site U1387, ranging from a depth of 90.72 meters composite depth (mcd) to 275.17 mcd. Sixty-nine samples were used from Site U1389, ranging from a depth of 156.14 mcd to 369.17 mcd. Site U1387 had a constant sedimentation rate of 27.5 cm/ky. Site U1389 had a sedimentation rate of 52.2 cm/ky above a widespread hiatus at 217.44 mbsf and 23.9 cm/ky below that hiatus.

Primary mineral phases include quartz, calcite, dolomite, aragonite, plagioclase, illite, a 7 Å clay, and various interstratified clays. Mineralogical data are consistent with the Expedition 339 shipboard XRD results, and onshore lithologies support an interpretation of local provenance. Compositional changes at the positions of the upper Mediterranean Outflow Water and the lower Mediterranean Outflow Water were considered during glacial and interglacial episodes, and variations were explained in terms of changes in weathering and in sediment transport paths.

Overall, there are no consistent variations in mineral abundances between glacial versus interglacial periods. This indicates that the Gulf of Cádiz contourite depositional system is complex, influenced by multiple controls.

ACKNOWLEDGMENTS

While I am very proud of my achievements as an undergraduate, there is no way I could have done it alone. I would like to thank Dr. Lawrence Krissek for his unlimited help and guidance throughout the past two years. He taught me the skills needed to conduct research and helped me create a better framework to approach analytical thinking. He trained me to constantly use my "Big Picture Glasses" and just between you, me, and a light post, I've inherited more idioms than one person should ever know. I would also like to thank Sean O'Brien for a successful collaboration during this project and for being the best teammate I've ever had.

Additionally, I am grateful to many other professors in the department. I would be lost without Dr. Julie Sheets. Her patience was endless and she spent many hours training me on the XRD equipment and software. Her methods for analyzing data and solutions to unexpected issues were instrumental in this project. Dr. Anne Carey was essential in my development of the skills needed to present a research project, create an abstract, and write a thesis. Witnessing her coordination of the Shell Undergraduate Research Experience was also valuable in gaining a further understanding of the practical mechanisms of research.

I am also appreciative of Shell Exploration & Production Company and SURE for their internship opportunity, USSSP for funding of XRD analysis, and IODP for providing samples. The OSU School of Earth Sciences Friends of Orton Hall provided the funds for travel, and the Marcus J. & Lottie C. Lieberman Scholarship in Geological Sciences helped finance my education.

Lastly, I would like to thank Tyler Wilson for his continuous inspiration and editorial support, and my parents for their love and encouragement during of all my endeavors, without whom, I would not be where I am today.

Introduction

Mediterranean Outflow Water (MOW) is a warm, saline bottom water current that begins in the Mediterranean Sea, flows out through the Strait of Gibraltar, sinks to a depth on the middle slope, and follows contours north along the West Iberian Peninsula (Figure 1).

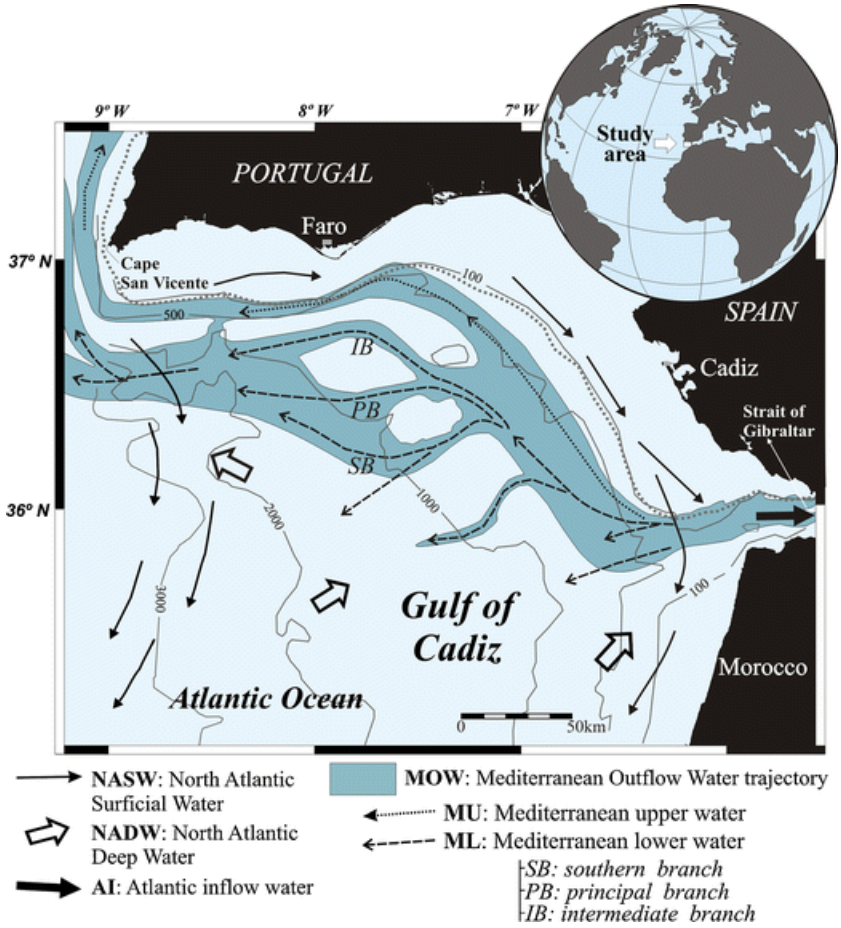

Figure 1: Locality map showing the main water mass circulation (Llave et al., 2011)

Because MOW is instrumental in this important Mediterranean-Atlantic water exchange, it directly affects the salinity of the North Atlantic Deep Water (NADW), and hence, increases the density of the Atlantic Meridional Overturning Circulation (AMOC), aiding in global thermohaline convection (Baringer and Price, 1999). See Figure 2 for a map of global thermohaline circulation. It

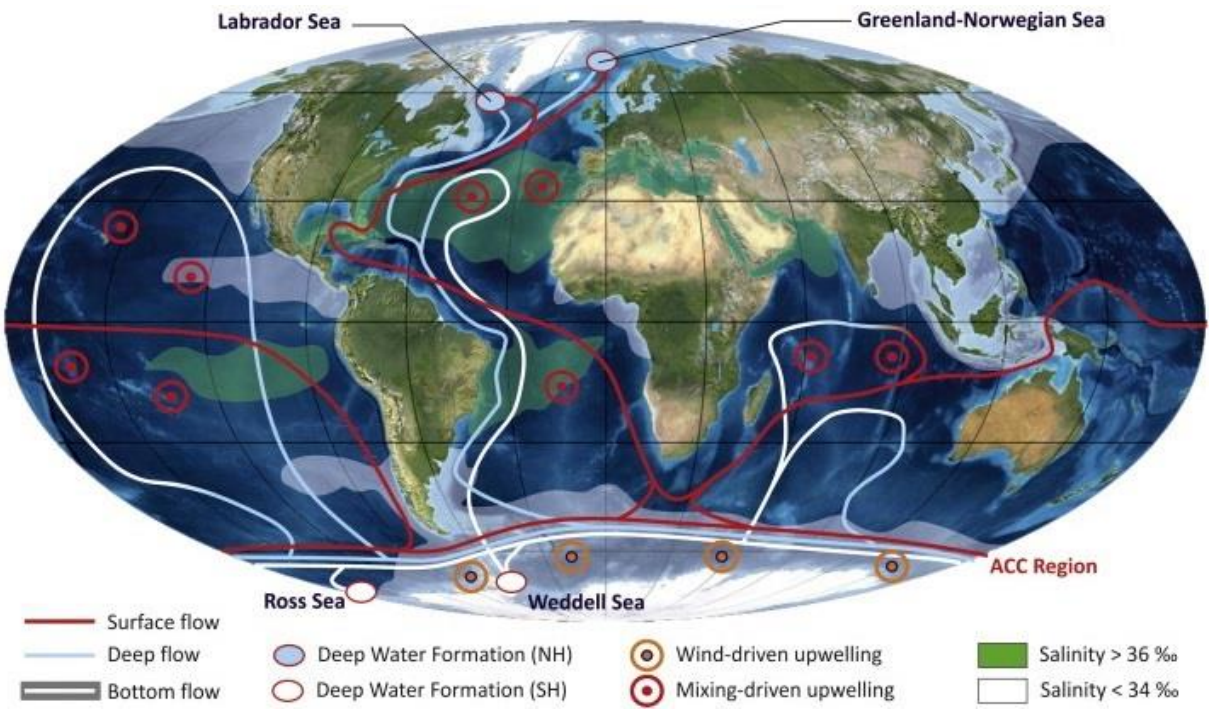

Figure 2: Global thermohaline circulation (Robesco et al., 2014)

is estimated that without MOW, AMOC would decrease by ~15% and North Atlantic sea surface temperatures would decrease by up to 1ºC (Hernandez-Molina et al., 2014b).

As MOW travels along the contours of the West Iberian Peninsula, it leaves evidence of its activity through bottom current deposits called contourites. The typical contourite facies (Figure 3) is described as having bi-gradational grading, abundant bioturbation, and a lack of clear lamination (Stow and Faugeres, 2008).

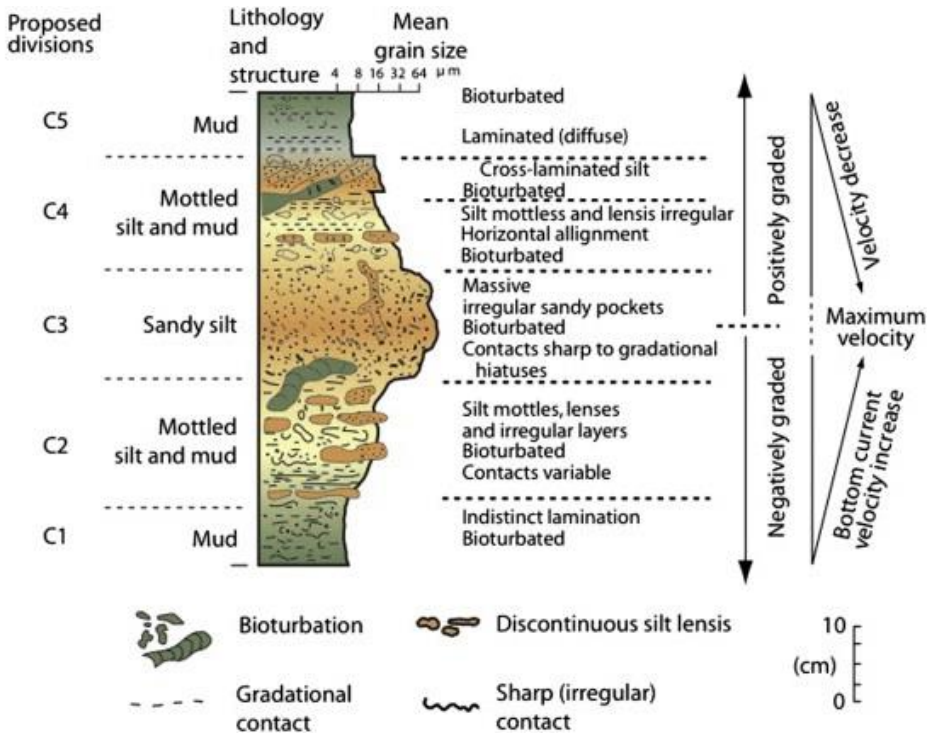

Figure 3: Contourite facies model (Stow and Faugeres, 2008)

Contourite deposits are characterized by unusually high sedimentation rates, allowing for high-resolution paleoceanographic studies (Bahr et al., 2014). Contourite study is important for paleoclimatology and paleoceanography, slope-stability and geological hazard assessment, and hydrocarbon exploration, due to their clean, well-sorted sands (Rebesco et al., 2014; Viana, 2008). Previous studies suggest that vertical variations in grain-size reflect MOW intensity, so coarse-grained deposits are inferred to represent periods of high MOW velocity and fine-grained deposits represent periods of low MOW velocity (Toucanne et al., 2007). Mineralogy also has the potential to be a useful proxy for determining MOW velocity variations and indicating terrestrial source and/or transport path by considering how mineral assemblages vary throughout time and space.

STUDY GOALS

Using core samples from Site U1387 and Site U1389, this study aimed to understand the history of Mediterranean Outflow Water and how it has changed through glacial and interglacial periods by analyzing sediment mineralogy, identifying compositional variations, and explaining any variations in terms of changes in weathering and sediment transport paths. This study utilized X-Ray Diffraction (XRD) analyses, in order to determine the bulk mineralogy of samples and to estimate mineral abundances relative to quartz. The potential causes of each mineral variation were then identified.

GEOLOGIC SETTING

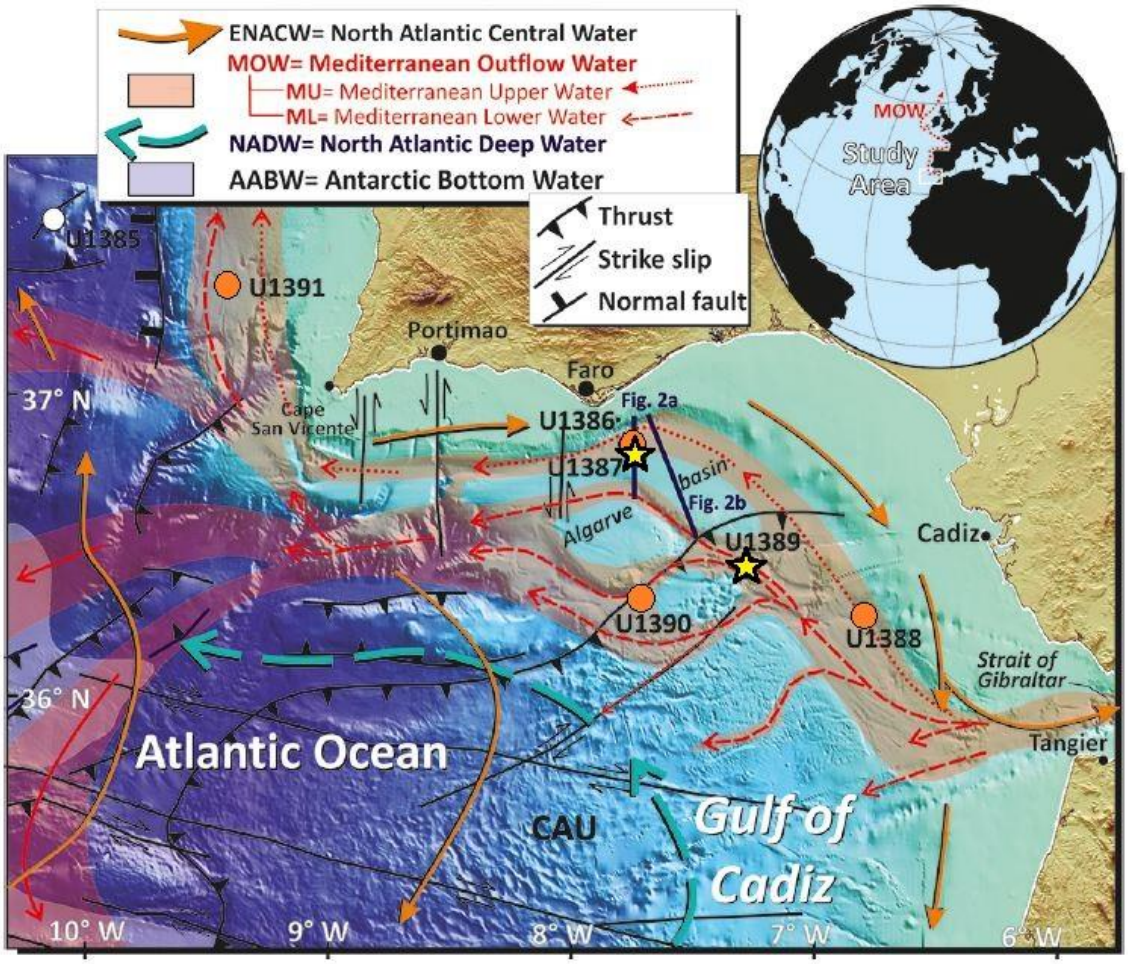

Figure 4: Locality map showing Expedition 339 sites and main water-mass circulation (Modified from Hernandez-Molina et al. 2013a)

The Gulf of Cadiz and West Iberian margin are the location of a complex contourite depositional system (Figure 4). Mediterranean Outflow Water (MOW) is a strong bottom current system that begins with its exit from the Strait of Gibraltar and flows toward the west and north-west due to the Coriolis force and margin bathymetry (Stow et al., 2013; Hernandez-Molina et al., 2008). The MOW is much warmer and more saline than other Atlantic Ocean water, so when the two bodies of water meet, the MOW sinks below the Atlantic water, due to a difference in density.

MOW flows above the North Atlantic Deep Water (NADW) and under Atlantic inflow, between 400 and 1400 meters below sea level (mbsl), and with a velocity of 300 cm/sec at the Strait of Gibraltar and 80-100 cm/sec at the latitude of Cape San Vicente (Hernandez-Molina et al., 2013a). The path of MOW closely follows the contours of the Gulf of Cadiz and splits into an upper core and a lower core on the middle slope (Figure 5). The upper core flows between approximately 500 and 700 mbsl and the lower core between 800 and 1400 mbsl (Hernandez et al., 2011).

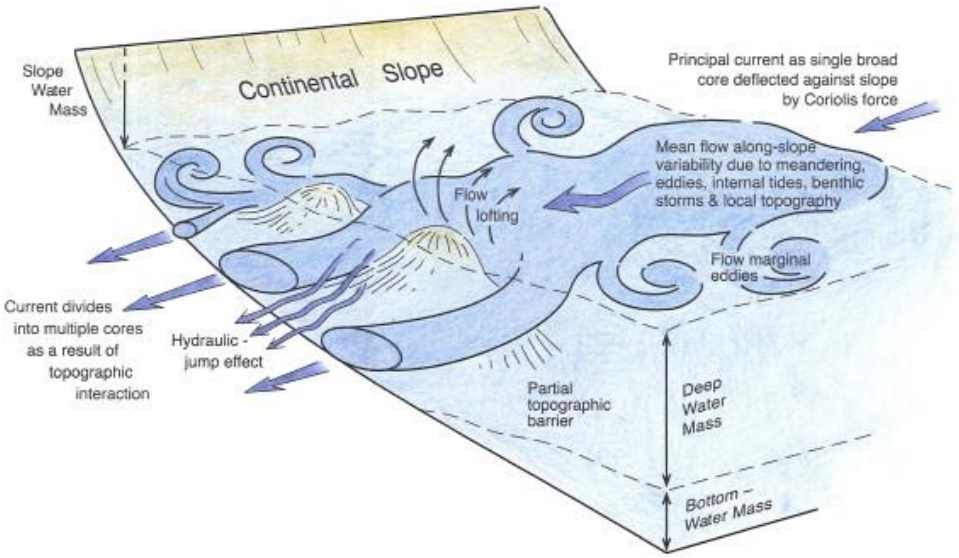

Figure 5: Diagram showing principal bottom-current features (Rebesco et al., 2014)

The main depositional features of the Gulf of Cádiz system are sedimentary wave fields, sedimentary lobes, mixed drifts, plastered drifts, elongated mounded and separated drifts, and sheeted drifts. The primary features caused by erosion are contourite channels, furrows, marginal valleys, and moats (Stow and Faugères, 2008). See Figure 6 for depositional and erosional features.

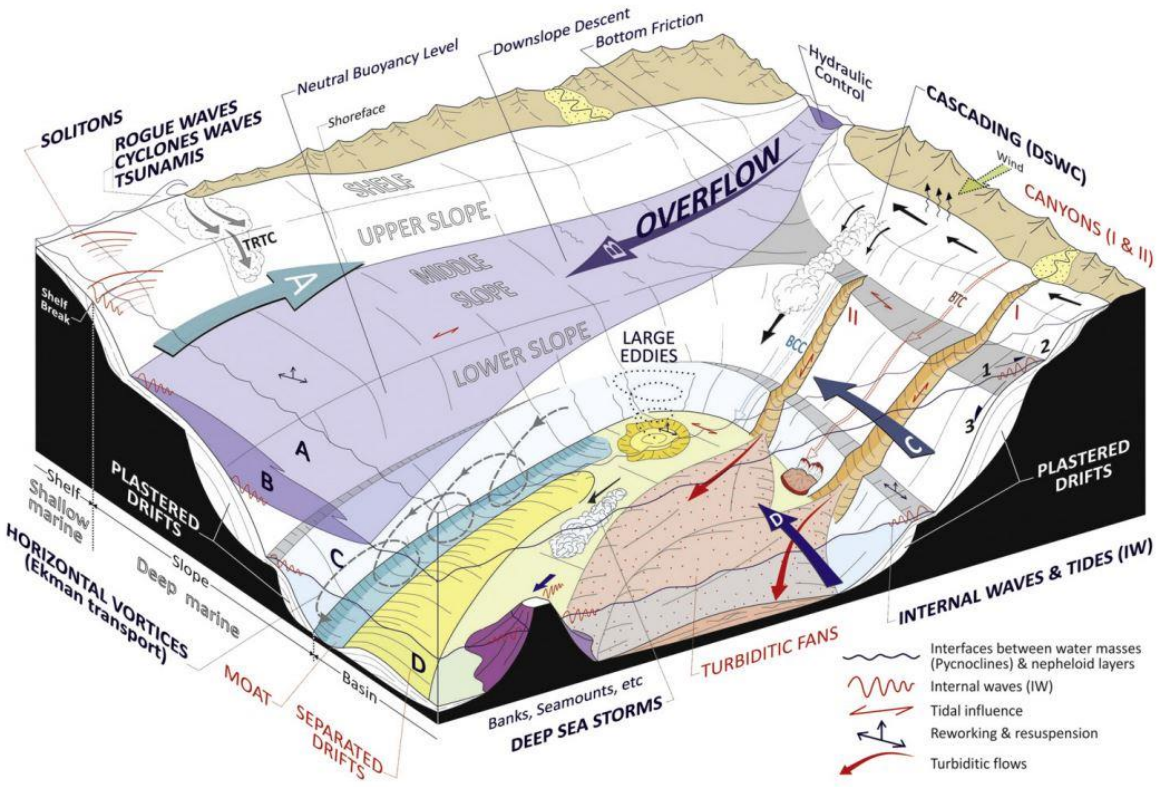

Figure 6: Depositional and erosional contourite features on the middle slope of the Gulf of Cadiz (Rebesco et al., 2014)

Currently, the upper core is the site of the stronger MOW flow, but this has not always been the case. In glacial periods of the past, the main flow of MOW has shifted to the lower core position (Hernandez-Molina et al., 2014a). In the present study, samples from the upper core and lower core of MOW are examined. Site U1387 (36º48.3210'N, 7º43.1321'W) is located in the upper terrace of the middle slope and was located to sample the MOW upper core. Site U1389 (36º25.515'N, 7º16.683'W) is located in the lower terrace of the middle slope and was located to sample the MOW lower core. Sediments at both sites consist of muddy, mottled silts and sandy contourites organized as bi-gradational sequences.

METHODS

Fifty-four samples were used from Site U1387, ranging from a depth of 90.72 meters composite depth (mcd) to 275.17 mcd. Sixty-nine samples were used from Site U1389, ranging from a depth of 156.14 mcd to 369.17 mcd. Average sample interval was 3.48 meters for Site U1387 and 3.05 meters for Site U1389. Site U1387 had a constant sedimentation rate of 27.5 cm/ky, so average sampling interval was 12.68 ky. Site U1389 had a sedimentation rate of 52.2 cm/ky above a widespread hiatus at 217.44 mbsf and 23.9 cm/ky below that hiatus, so average sampling interval was 6.36 ky above the hiatus and 12.41 ky below it. Sample age was determined using a shipboard age/depth model based on paleomagnetic and biostratigraphic data as shown in Figure 7 and Figure 8.

Samples were ground by hand using a mortar and pestle. Sediment was back-loaded as a powder into a randomly oriented mount and analyzed using x-ray diffractometry (XRD). An average of 0.7607 grams of sample was used per mount. The PANalytical X'Pert Pro XRD in the Subsurface Energy Materials Characterization & Analysis Laboratory (SEMCAL) in the School of Earth Sciences at Ohio State University was used for analysis. Samples were scanned using Ni-filtered CuKα radiation. A step size of 0.020º2θ was used from 4.0-70.0º at 2 sec/step. Tension was set to 45 kV and current to 40 mA. Incident beam optics were 1, 2 and diffracted beam optics were 2, 1.

The PANalytical HighScore (Plus) program and Data Viewer were used to determine the background of XRD patterns. Background in HighScore (Plus) was determined using a granularity of 20 and a bending factor of 2. Peaks were searched with a minimum significance of 1.00, minimum tip width of 0.10, maximum tip width of 1.00, and peak base width of 2.00. After the automated search was complete, unmarked peaks were inserted manually. The Search and Match feature of HighScore (Plus) was used to determine what mineral phases were present (see Figure 9).

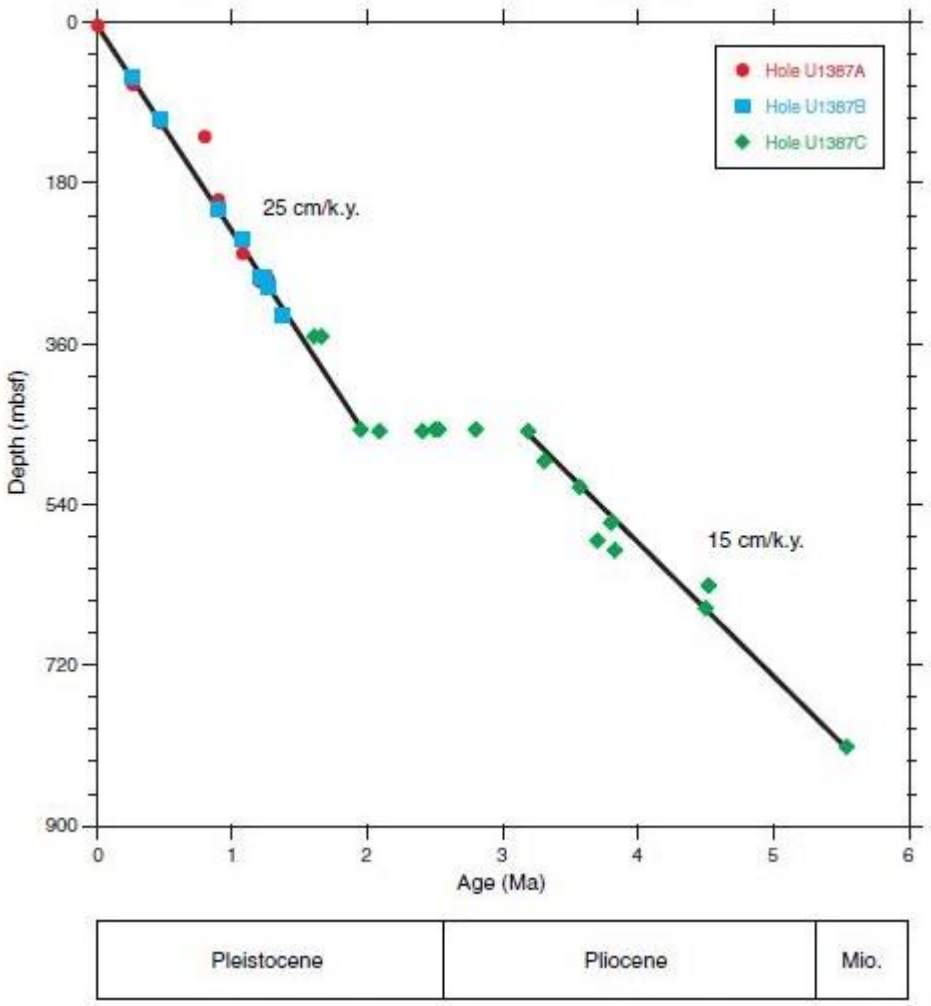

Figure 7: Biostratigraphic events vs. depth, Site U1387 (Hernandez-Molina et al, 2013b)

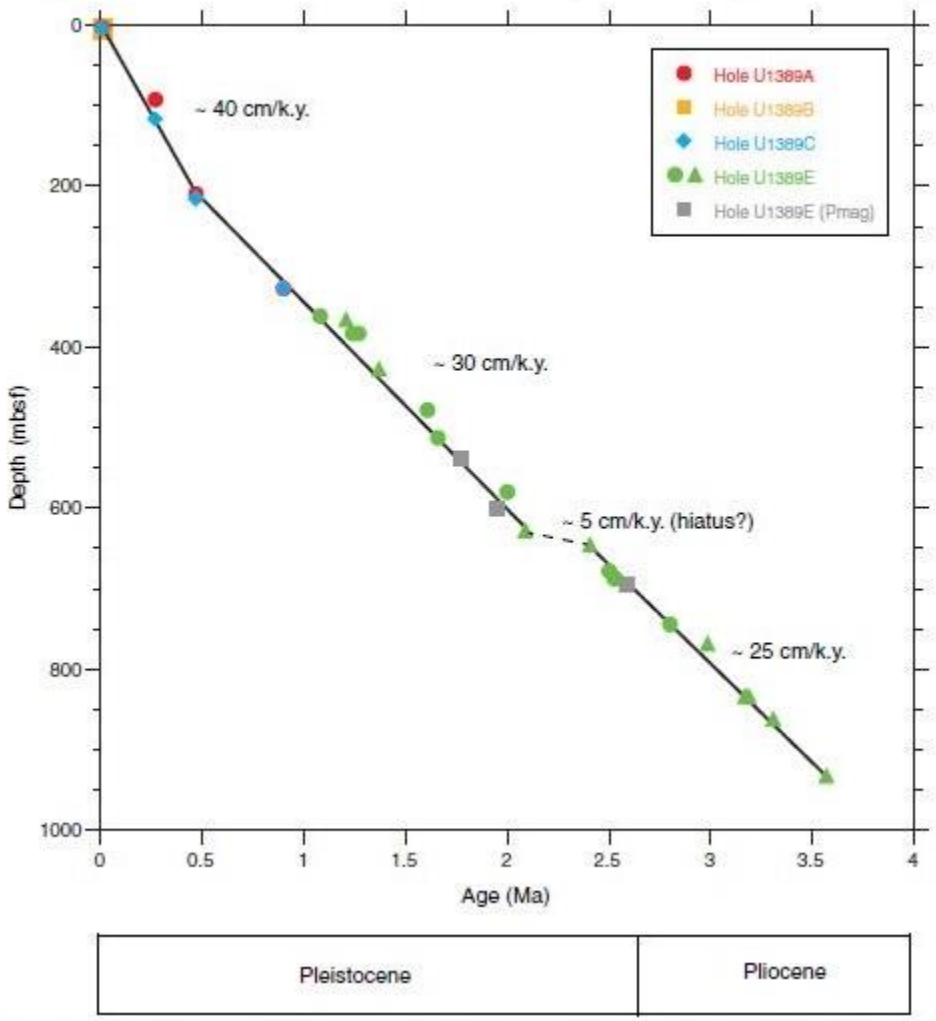

Figure 8: Biostratigraphic events vs. depth, Site U1389 (Hernandez-Molina et al, 2013b)

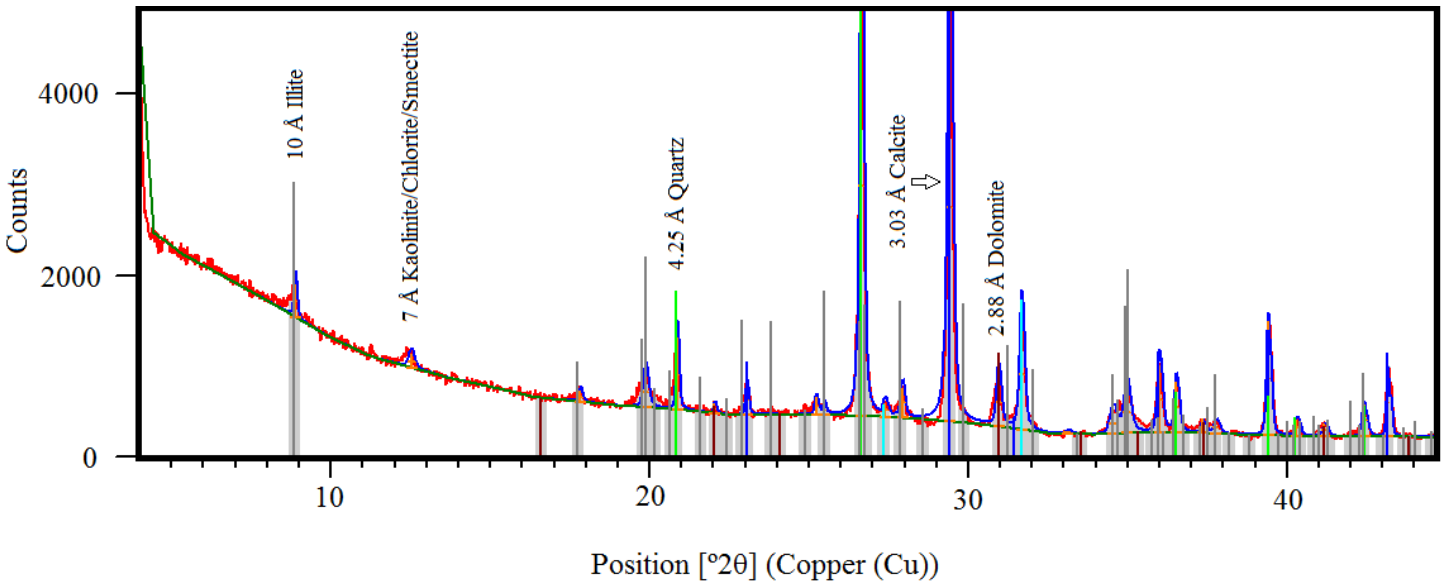

Figure 9: Example of an x-ray diffraction pattern from Site U1387, with key mineral phases identified via HighScore (Plus)

Unrecognized peaks were identified manually, using "Table of Key Lines in X-ray Powder Diffraction Patterns of Minerals in Clays and Associated Rocks" (Chen, 1977) and "Identification of Clay Minerals by X-ray Diffraction Analysis" (Brindley, 1955). A HighScore (Plus) default profile fit was run on each diffraction pattern to estimate the area of a key peak for each mineral. See Appendix F for Data Collector and HighScore (Plus) standard operating procedures. Due to their low intensity and steep background, the areas of the clay peaks (illite and the 7 Å clay) had to be estimated using the Data Viewer program. This was done by opening the XRD pattern in Data Viewer and manually gathering peak areas using the Peak Parameters function. Backgrounds of clay peaks were determined by eye. Key peaks for each mineral were as follows: calcite (3.03 Å), dolomite (2.88 Å), quartz (4.25 Å), illite (10 Å), and kaolinite/chlorite/smectite (7 Å). These peaks were chosen in order to minimize the amount of overlap with other minerals. Example XRD patterns are shown in Appendix E.

The area of each mineral's peak was normalized relative to the area of the quartz peak from that pattern. Ratios of each mineral peak area/quartz peak area were grouped according to Marine Isotope Stage (Lisiecki and Raymo, 2005a) and then averaged. See Appendix A for IODP sample list and Appendix B for sample groupings at each site. See Table 1 for MIS boundaries and associated ages. This study provides a semiquantitative estimate of mineral abundances, so abundances cannot be compared between the different minerals. Instead, the relative abundance of each mineral could be compared over time, and could be used to identify covarying mineral assemblages.

Replicates were analyzed for 10% of samples in order to determine analytical uncertainties. These uncertainties are listed in Table 2 for each site.

TABLE 1

Ages of MIS Boundaries

MIS Boundary	Age (ka)
8/9	300
9/10	337
10/11	374
11/12	424
12/13	478
13/14	533
14/15	563
15/16	621
16/17	676
17/18	712
18/19	761
19/20	790
20/21	814
21/22	866
22/23	900
23/24	917
24/25	936
25/26	959
26/27	970
27/28	982
28/29	1014

(Lisiecki and Raymo, 2005b)

TABLE 2

Analytical Uncertainty in Intensity Ratios – Site U1387

Mineral	Diffraction Peak (Å)	Uncertainty (%)
Calcite	3.03	±2.64
Dolomite	2.88	±10.12
Illite	10	±9.93
Kaolinite/Chlorite/Smectite	7	±7.23
Quartz	4.25	±2.45

Analytical Uncertainty in Intensity Ratios – Site U1389

Mineral	Diffraction Peak (Å)	Uncertainty (%)
Calcite	3.03	±8.12
Dolomite	2.88	±8.67
Illite	10	±14.54
Kaolinite/Chlorite/Smectite	7	±8.49
Quartz	4.25	±5.43

Uncertainties were calculated for each mineral (except quartz) as the average of:
[(maximum peak area ratio – mean peak area ratio)/mean peak area ratio]*100

For quartz, the uncertainty is the average of:
[(maximum peak area – mean peak area)/mean peak area ratio]*100

RESULTS

The major mineral phases that are present at Site U1387 and Site U1389 are quartz, calcite, dolomite, aragonite, plagioclase, illite, a 7 Å clay, and various interstratified clays. Identification of the 7 Å clay was not possible in this study, since glycolation of samples was not performed. Therefore, the 7 Å peak can only be identified as kaolinite and/or chlorite and/or smectite.

Figures 10(a-e) and 11(a-e) display mineral intensity ratios through time at each site, averaged for each Marine Isotope Stage, and the average intensity of the 4.25 Å quartz peak. Table 3 lists the average ratio values by Marine Isotope Stage for each site and an indication of average values whose change relative to the underlying MIS is within analytical uncertainty. Mineral peak areas are presented in Appendix C for all samples and mineral/quartz ratios are presented in Appendix D.

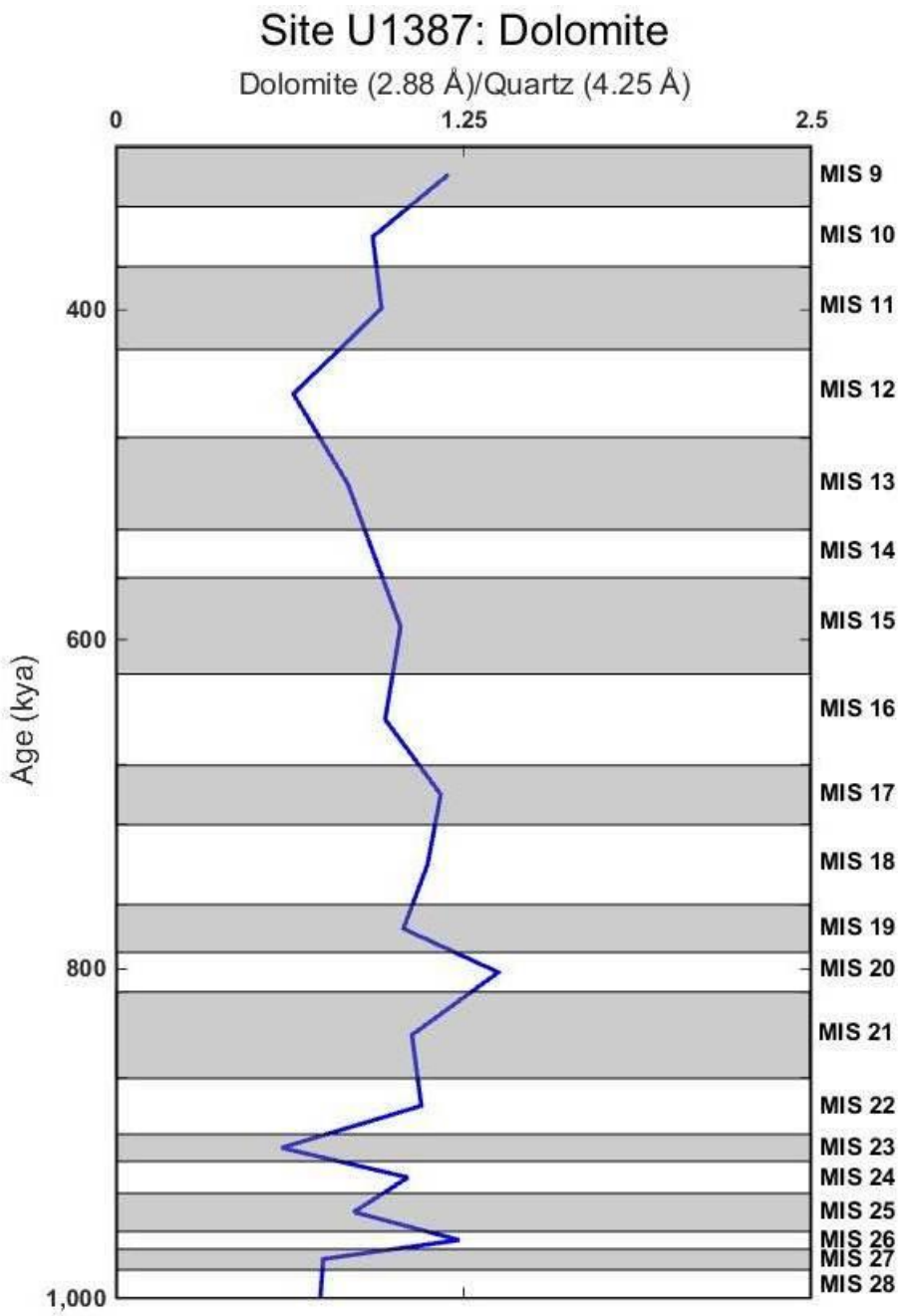

Figure 10a: Intensity ratios of dolomite, relative to quartz at Site U1387, upper core MOW

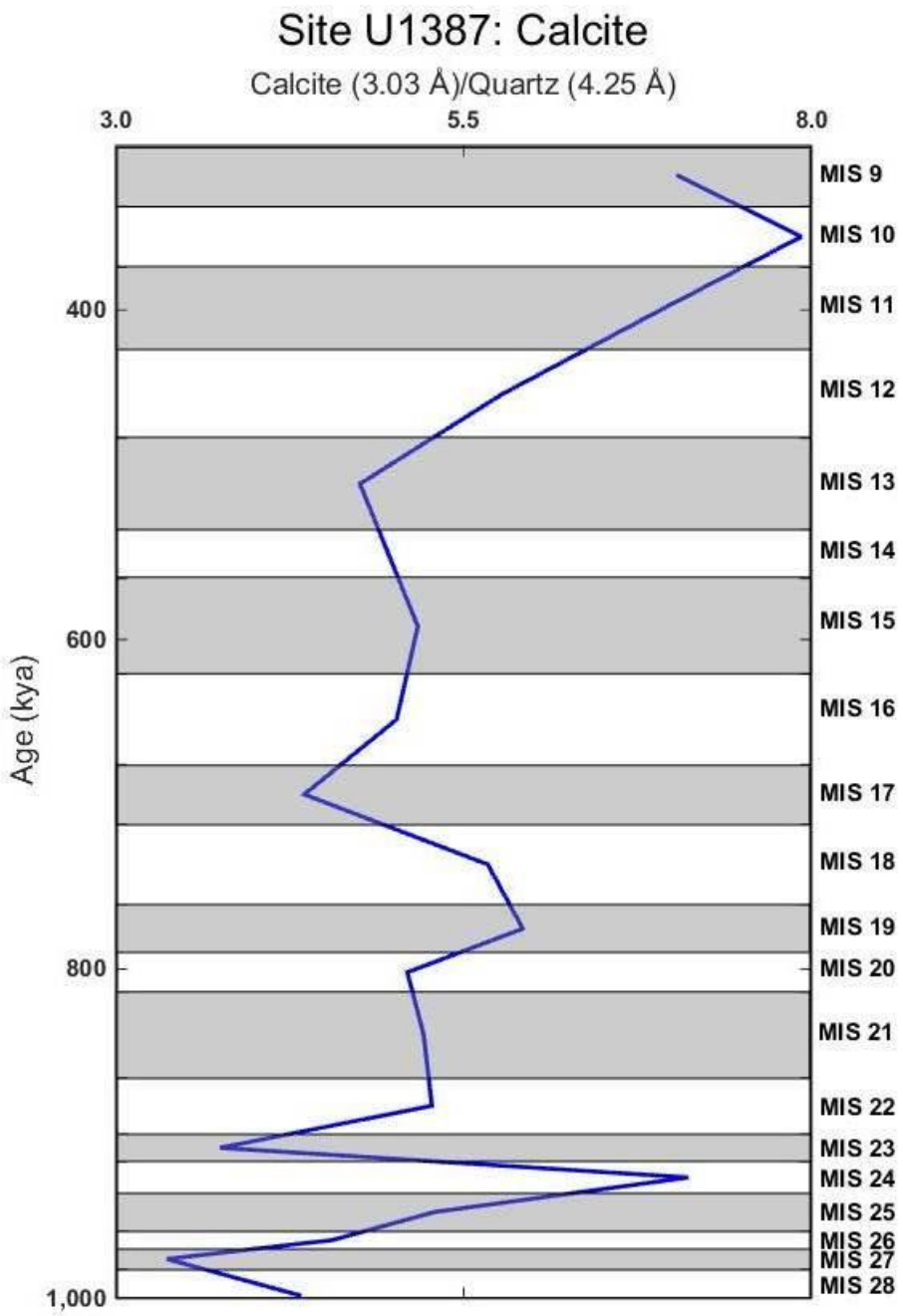

Figure 10b: Intensity ratios of calcite, relative to quartz at Site U1387, upper core MOW

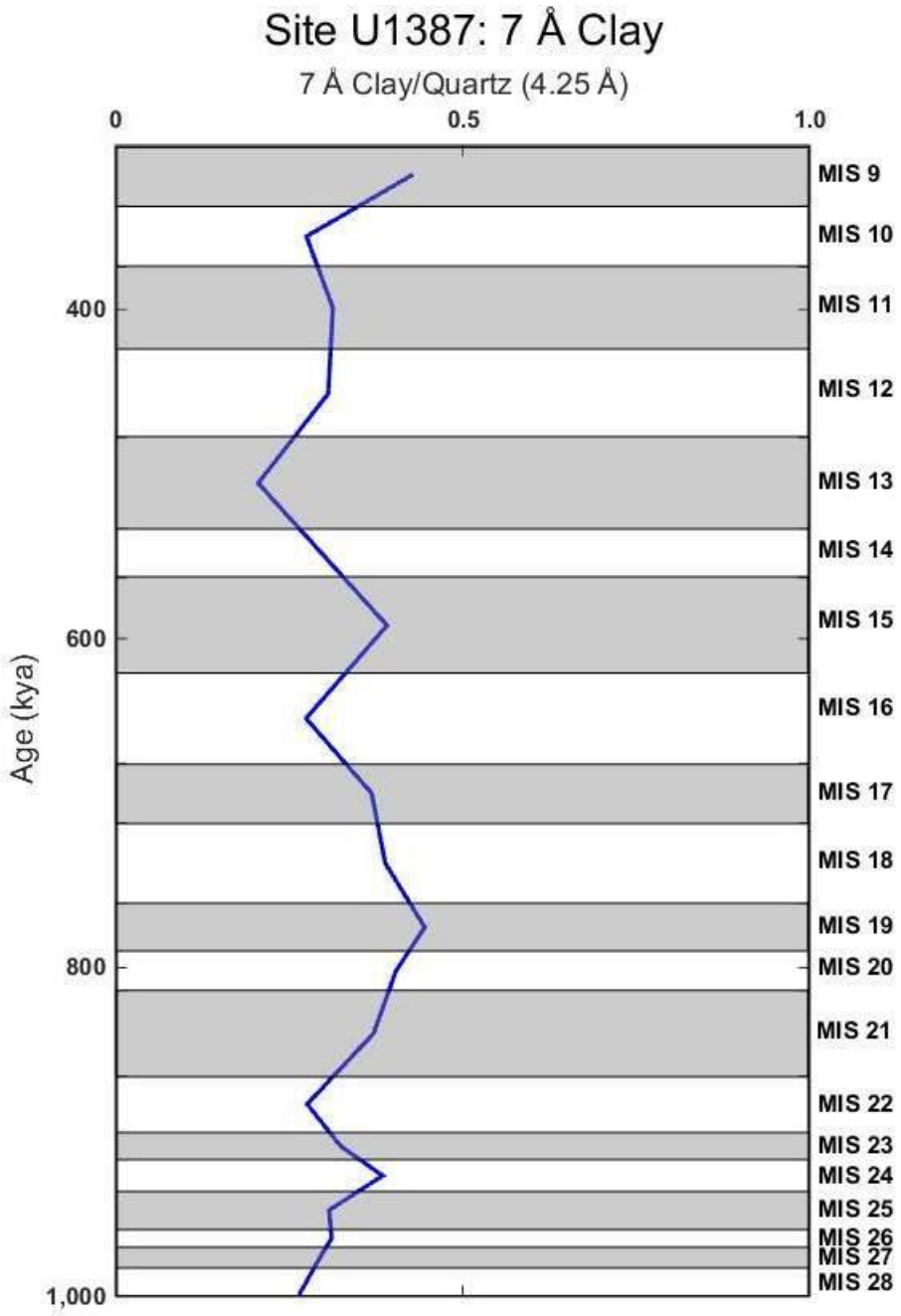

Figure 10c: Intensity ratios of 7 Å clay, relative to quartz at Site U1387, upper core MOW

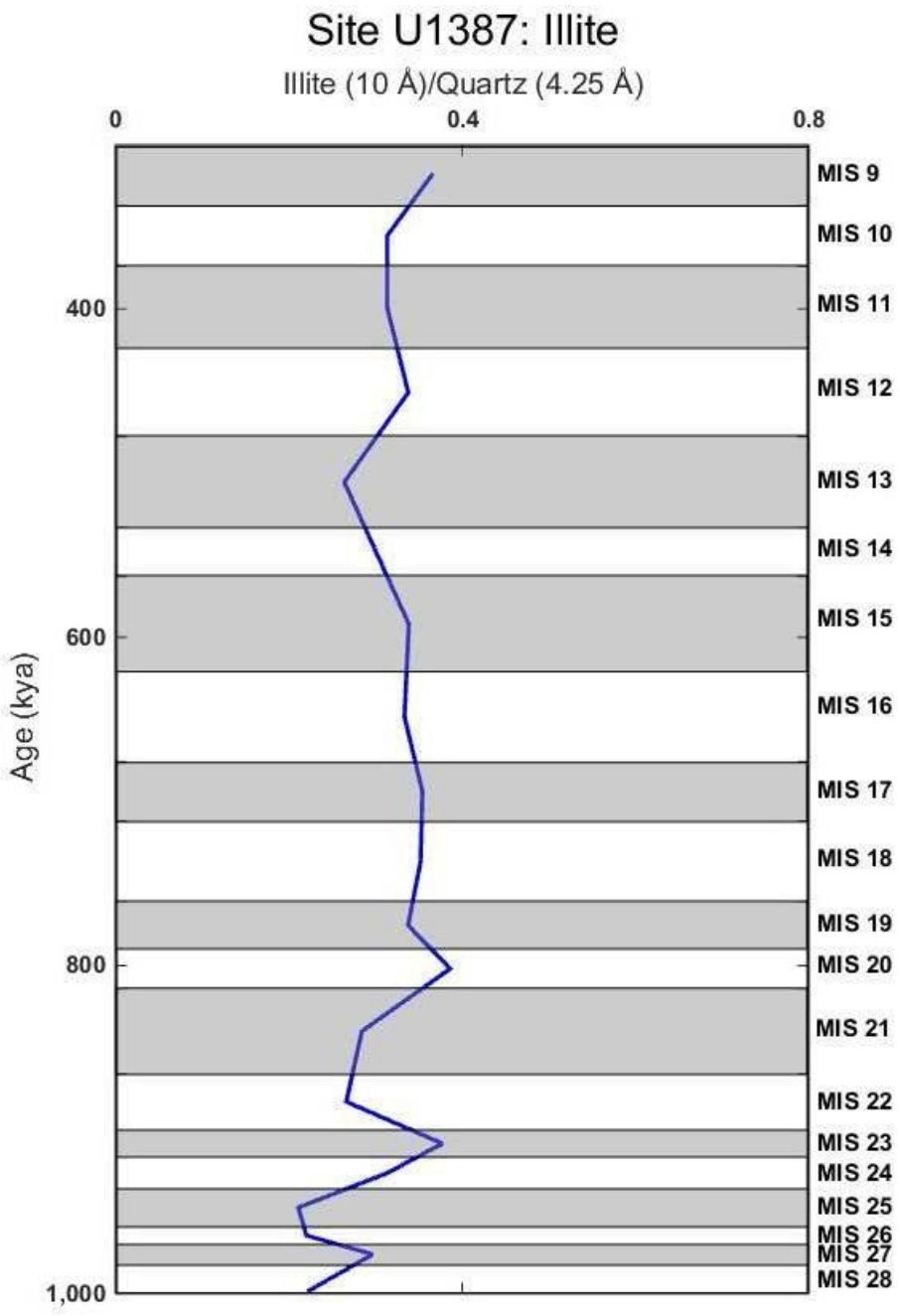

Figure 10d: Intensity ratios of illite, relative to quartz at Site U1387, upper core MOW

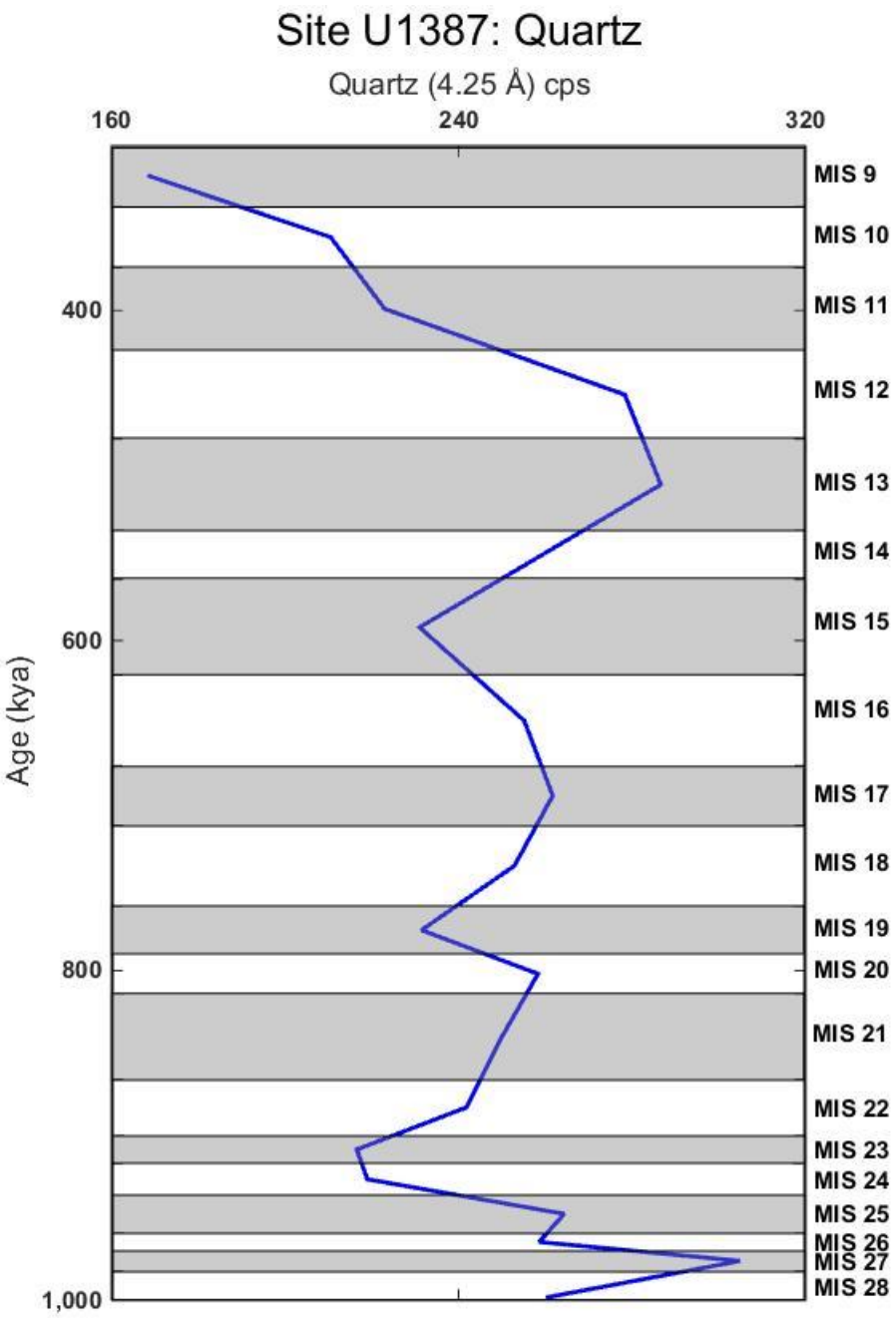

Figure 10e: Areas of quartz peak at Site U1387, upper core MOW

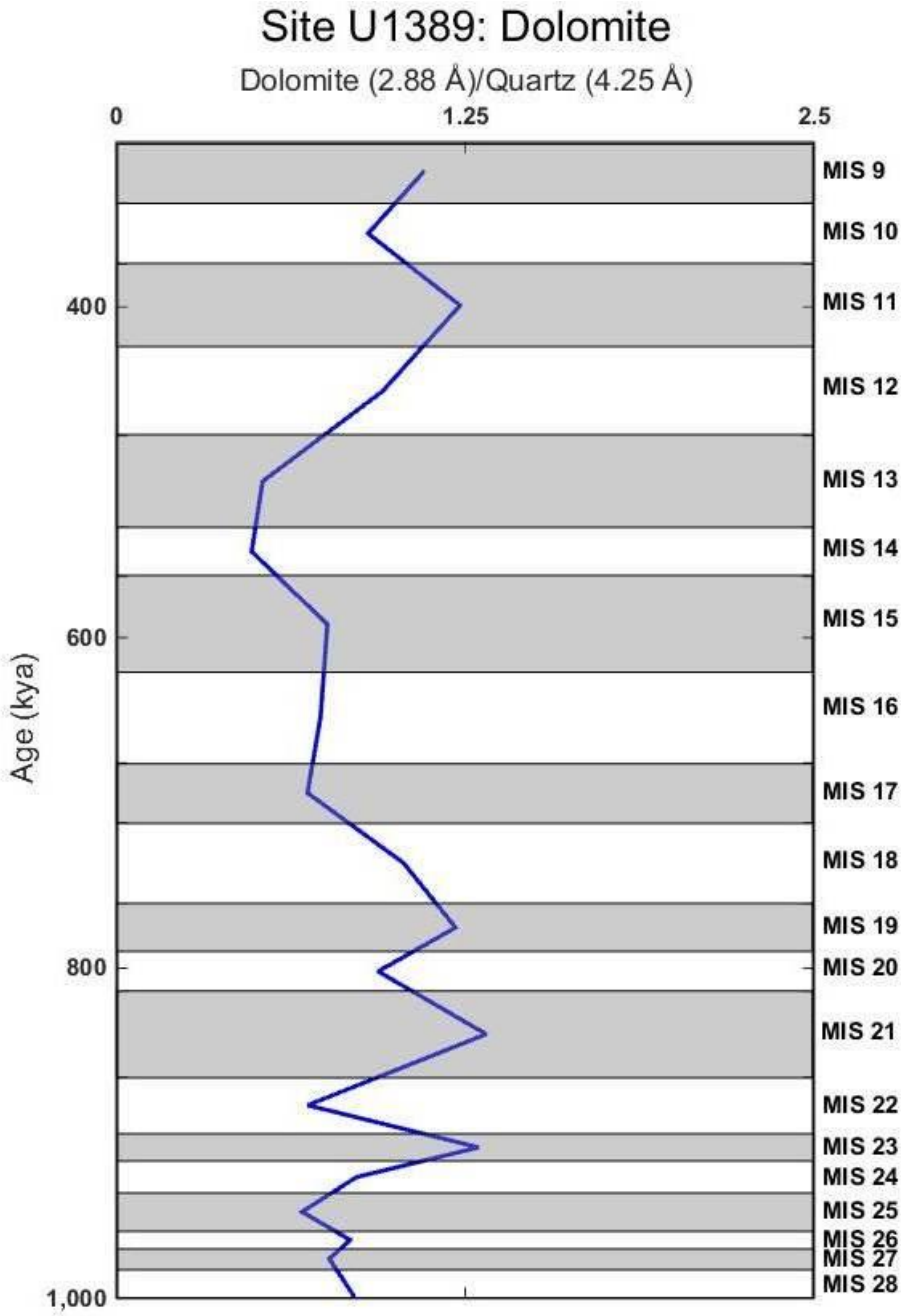

Figure 11a: Intensity ratios of dolomite, relative to quartz at Site U1389, lower core MOW

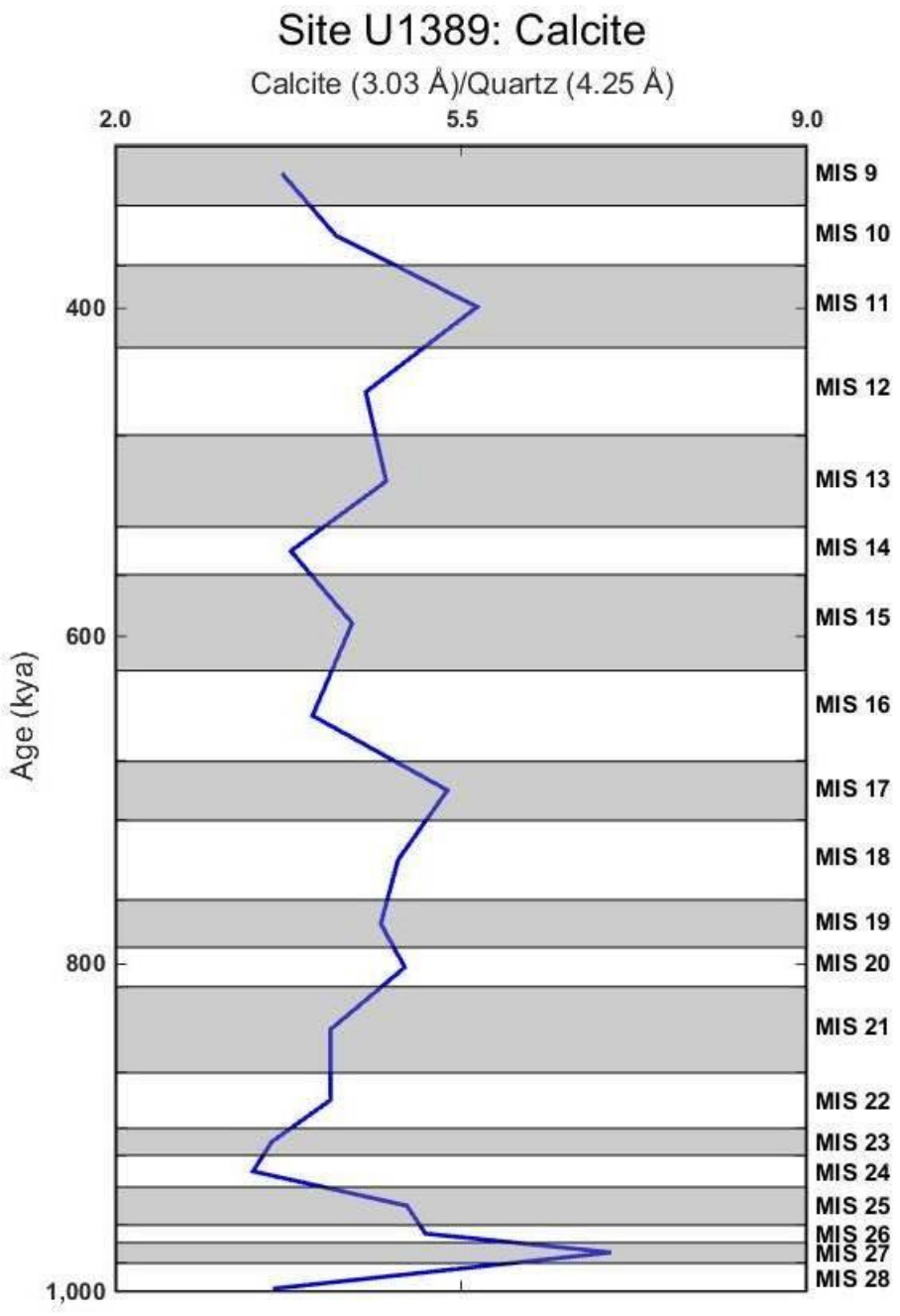

Figure 11b: Intensity ratios of calcite, relative to quartz at Site U1389, lower core MOW

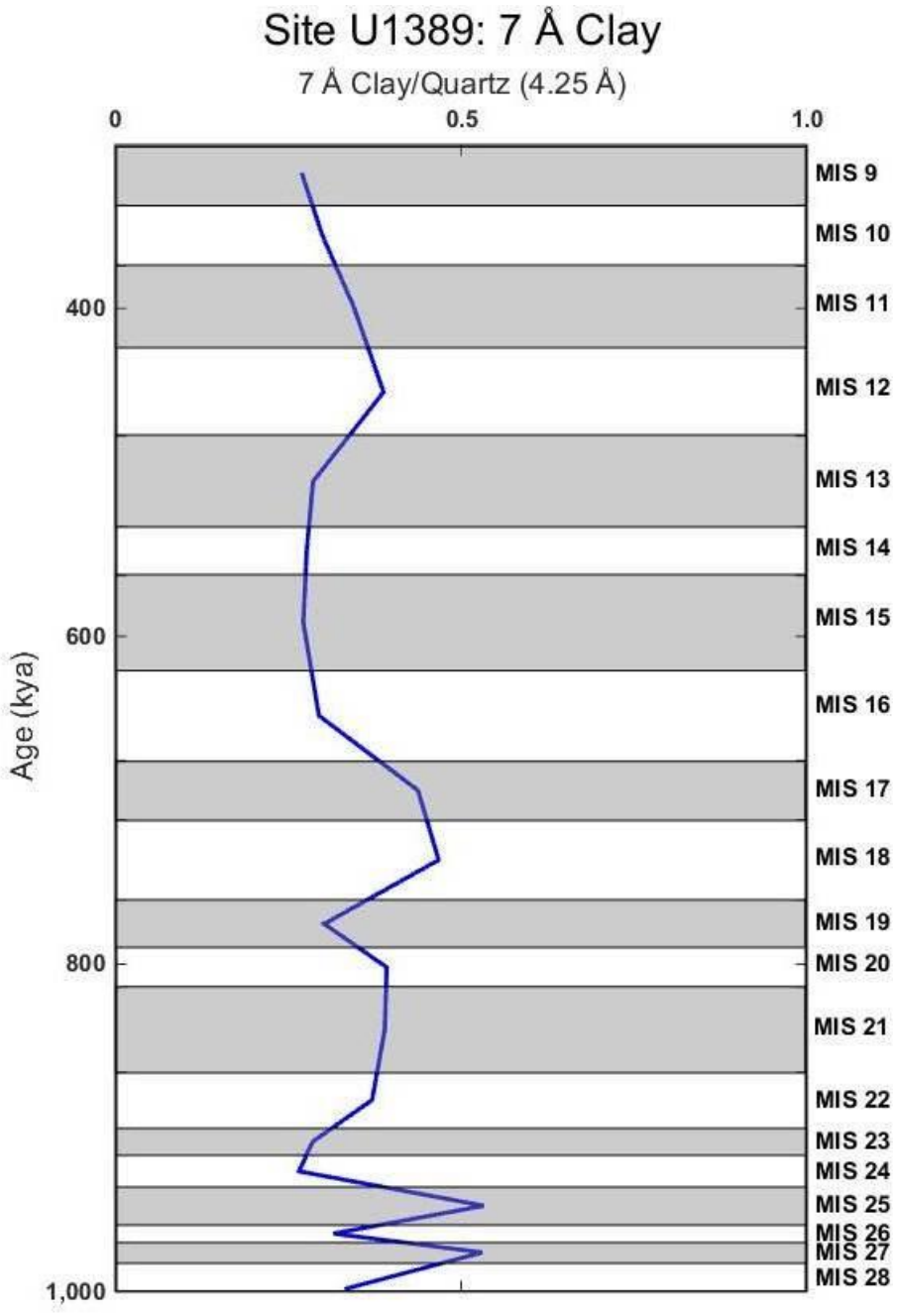

Figure 11c: Intensity ratios of 7 Å clay, relative to quartz at Site U1389, lower core MOW

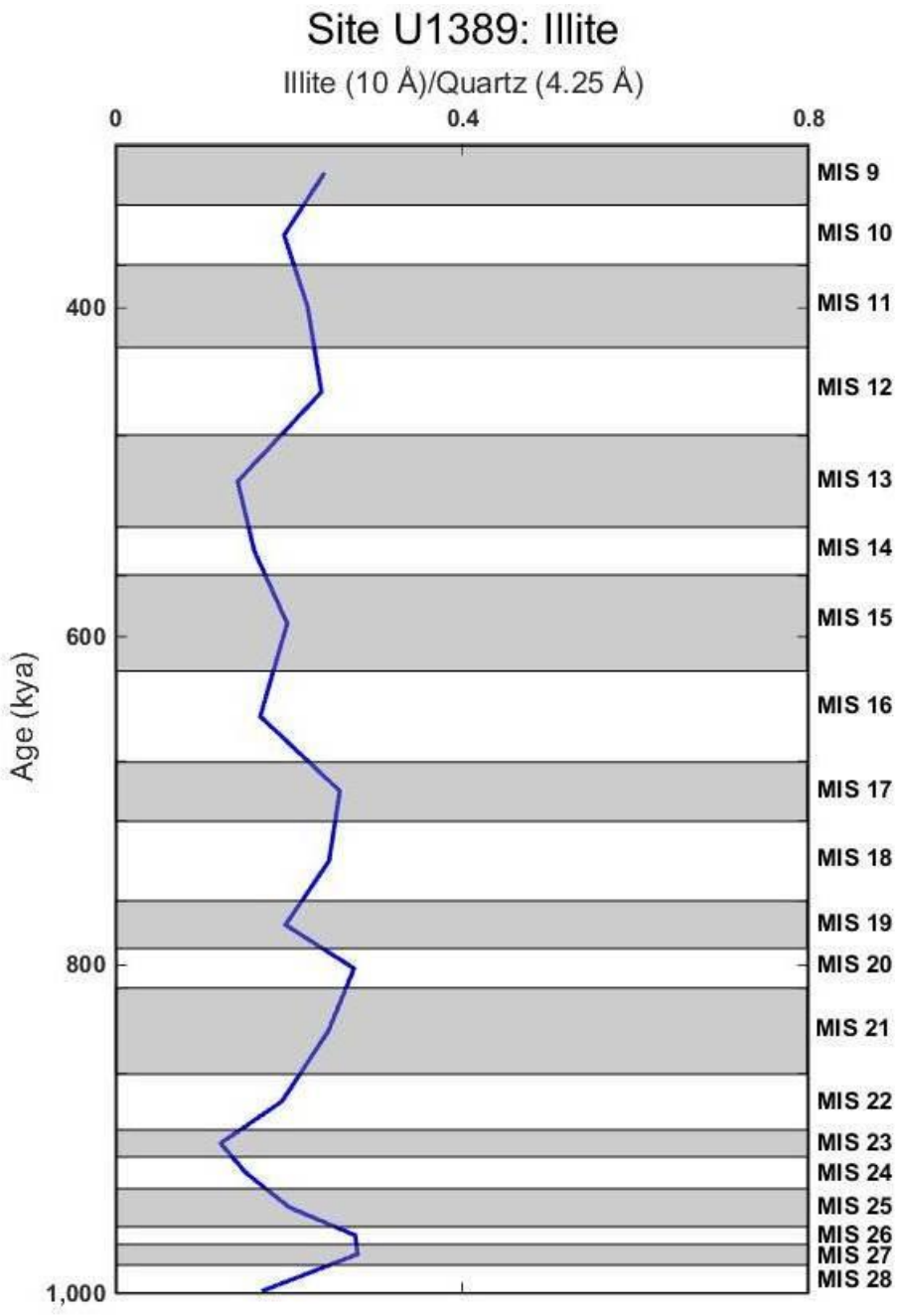

Figure 11d: Intensity ratios of illite, relative to quartz at Site U1389, lower core MOW

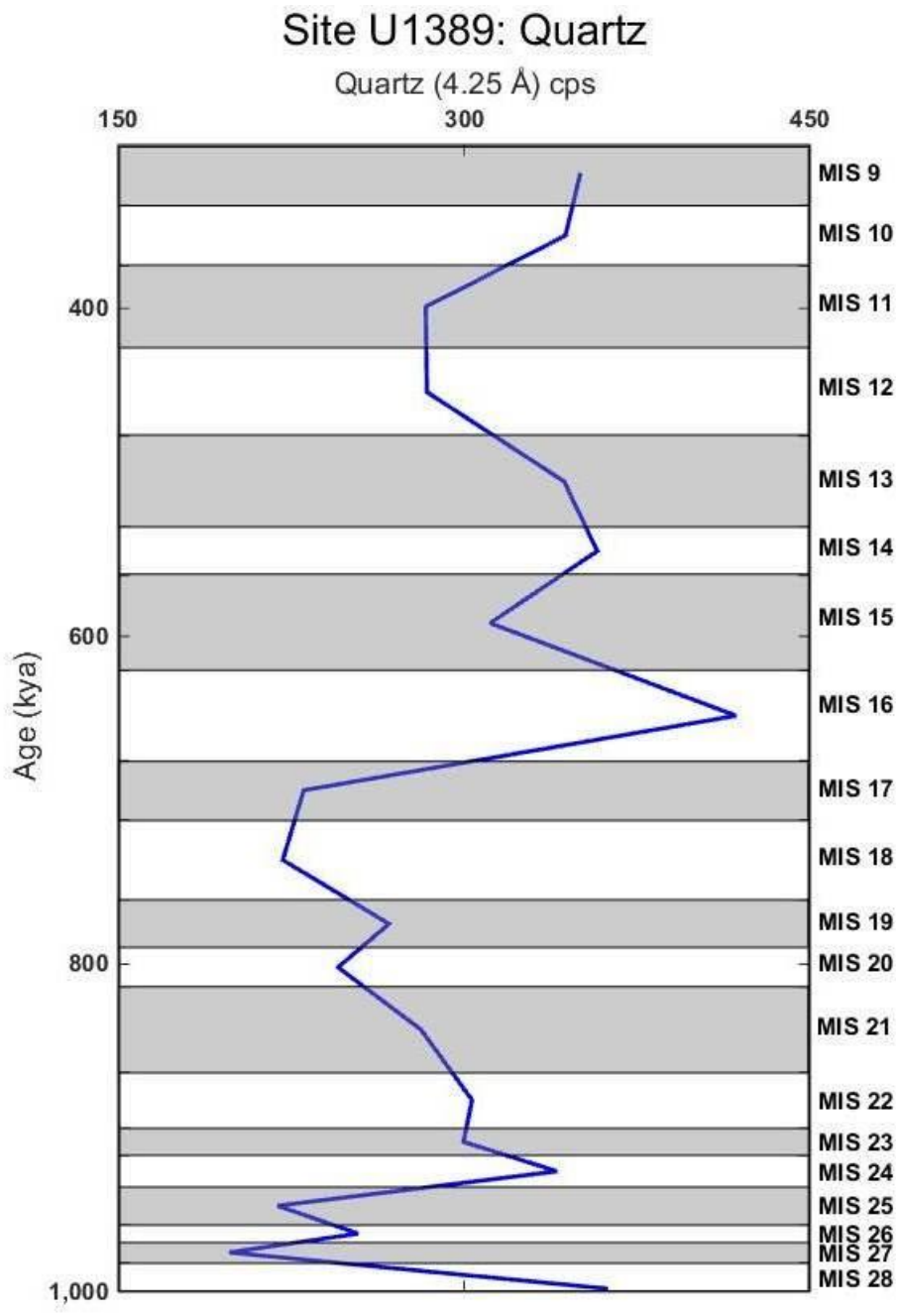

Figure 11e: Areas of quartz peak at Site U1389, lower core MOW

TABLE 3

Marine Isotope Stage Averages – Site U1387

MIS	Calc/Qtz	Dolo/Qtz	Ill/Qtz	7 Å/Qtz	Qtz
$9_{(n=1)}$	7.04	1.19	*0.36	0.43	168.78
$10_{(n=1)}$	7.93	*0.92	*0.31	*0.28	210.51
11	6.94	0.95	*0.31	*0.31	222.99
12	5.78	0.64	0.34	0.31	*278.30
13	4.76	0.83	0.26	0.21	286.60
14		No Samples			
15	*5.17	*1.02	*0.34	0.39	231.02
16	5.02	*0.97	*0.33	0.27	*255.11
17	4.35	*1.17	*0.35	*0.37	*261.70
18	*5.67	*1.12	*0.35	*0.39	252.88
19	5.92	1.03	*0.34	*0.45	231.48
20	*5.10	1.37	0.39	*0.40	*258.29
21	*5.21	*1.06	*0.28	0.37	*250.03
22	5.27	1.10	0.27	0.28	241.75
$23_{(n=1)}$	3.75	0.60	0.38	*0.32	*216.54
24	7.11	1.05	0.31	0.38	218.98
25	5.29	0.86	*0.21	*0.31	*264.32
$26_{(n=1)}$	4.56	1.23	0.22	*0.31	258.57
$27_{(n=1)}$	3.37	*0.75	0.30	*0.29	304.88
28	4.32	0.74	0.22	0.27	260.58

*Change from average value in underlying MIS is within analytical uncertainty

Marine Isotope Stage Averages – Site U1389

MIS	Calc/Qtz	Dolo/Qtz	Ill/Qtz	7 Å/Qtz	Qtz
9	*3.70	1.10	*0.24	*0.27	*350.25
10	4.23	0.90	*0.19	*0.30	343.94
11	5.66	1.23	*0.22	*0.34	*283.36
12	*4.54	0.95	0.24	0.39	283.91
13	4.74	*0.52	*0.14	*0.29	*343.32
14	*3.78	0.49	*0.16	*0.28	357.73
15	*4.40	*0.76	*0.20	*0.27	311.32
16	4.00	*0.73	0.17	0.29	417.90
17	*5.36	0.69	*0.26	*0.44	*230.52
18	*4.86	*1.03	*0.25	0.47	221.40
19	*4.69	1.22	0.20	0.30	*267.46
20	4.93	0.94	*0.28	*0.39	245.37
21	*4.18	1.33	*0.25	*0.39	*281.30
22	*4.18	0.69	0.19	0.37	*303.45
$23_{(n=1)}$	*3.58	1.30	*0.12	*0.29	299.76
$24_{(n=1)}$	3.40	0.86	*0.15	0.27	340.33
$25_{(n=1)}$	*4.95	0.67	0.20	0.53	219.19
$26_{(n=1)}$	5.14	*0.84	*0.28	0.32	254.07
$27_{(n=1)}$	7.02	*0.76	0.28	0.53	198.23
28	3.62	0.85	0.17	0.33	361.45

*Change from average value in underlying MIS is within analytical uncertainty

Discussion

In the preceding Results section, mineral intensity ratios were grouped by MIS, averaged per stage, and plotted at the midpoint of each MIS age range. Figures 10(a-e) and 11(a-e) display average mineral intensity ratios through time at each site and the average intensity of the 4.25 Å quartz peak area. As discussed below, several of the mineral abundance plots show different patterns above and below Marine Isotope Stage 16. In order to see how individual minerals varied during glacial and interglacial periods at each site, average values for glacial periods and for interglacial periods younger than MIS 16 and for MIS 16 and older, are examined. The overall mineral changes between sites then are considered.

Overall, the mineral abundances display different patterns above and below Marine Isotope Stage 16. At Site U1387, younger than MIS 16, quartz has a unique pattern, not covarying with any other mineral (Figure 10e). The 7 Å clay and illite generally covary, and exhibit a weak association with dolomite (Figures 10c, 10d, and 10a, respectively). Calcite exhibits its own pattern (Figure 10b). Below MIS 16, quartz and dolomite covary. The 7 Å clay and illite generally covary, but are a bit offset from each other. The clays and calcite exhibit a weak association, although the 7 Å clay covaries more with calcite than illite does. At Site U1389, calcite and illite covary, especially below MIS 14. Calcite and dolomite covary above MIS 16, but display an inverse correlation below MIS 16. Quartz and dolomite are inversely correlated.

The abundances of individual minerals generally do not show a consistent pattern of relative highs or lows through the complete sequence of glacial and interglacial periods at each site (Table 4). At Site U1387, illite, the 7 Å clay, and quartz exhibit no consistent pattern of increased or decreased abundances during glacials and interglacials. Average calcite abundances are higher in glacial periods and lower during interglacials. This is true above and below MIS 16. Above MIS 16, dolomite is

more abundant during interglacial periods and less abundant during glacial periods. Below MIS 16, however, the dolomite abundance pattern is reversed, with higher abundances during glacial periods than during interglacials. At Site U1389, illite, the 7 Å clay, and quartz show no consistent pattern of abundances through the full record of glacials and interglacials. Calcite has relative highs during interglacial periods above MIS 17, lows during interglacials between MIS 19-23, and highs during interglacials from MIS 24-28. Dolomite displays relative highs during interglacial periods from MIS 18-24, but does not show a consistent pattern relative to glacial and interglacial periods in the rest of the record.

Another important aspect to consider is how mineral abundances at the two sites compare at specific times. When comparing sediments of the same age at Sites U1387 and U1389, calcite abundances show an inverse correlation below MIS 16. Dolomite abundances also exhibit an inverse correlation from MIS 16 through MIS 24. The 7 Å clay abundances show a weak inverse relationship during MIS 13-16 and MIS 18-22. Illite shows a covarying pattern between the two sites. Above MIS 16, quartz displays a covarying pattern, but below MIS 16 it displays an inversely correlated pattern.

Overall, the assemblages and relative abundances of minerals at Sites U1387 and U1389 vary in both space and time, are not the same at each site over time, and do not consistently covary—either positively or inversely—at the two sites at the same time (Table 5). There are few or no consistent variations in mineral abundances for the full record of glacial versus interglacial periods at either site. Some patterns of variation do exist for parts of each record, but those patterns differ above and below ~MIS 16, and patterns are more pronounced below MIS 16. If mineralogic variations were strongly controlled by sediment grain size, as suggested by limited previous work on Site U1387 (O'Brien, 2014) then sediment composition should be directly influenced by the

changing position of the core of MOW during glacials vs. interglacials. Because this consistent pattern is not observed, then either mineral supply was not consistent for all glacials and interglacials, the position of the MOW core was not always shallower during interglacials and deeper during glacials, or other variables were important. Sediment supply could have been varying in a complex way through glacial/interglacial episodes. For example, multiple sources could have supplied sediment to the region, with the relative importance of each source changing through time. The Guadiana, Tinto-Odiel, Guadalquivir, and Guadalete rivers all could have contributed to the sediment supply, but in proportions that varied through time (Gibbons and Moreno, 2002). Quartz could have been supplied by rivers, or could have been wind-blown from Africa. Calcite could have been supplied both from land and from marine organisms, which further complicates the likelihood that calcite abundances would respond in a simple fashion to shifts in MOW position. Another potential complication is diffuse downslope movement. This could have occurred along the margin and caused mixing of sediment between the upper and lower cores. The Gulf of Cádiz contourite depositional system is complex, having many influences. As a result, mineralogy alone is not a sensitive-enough proxy to map MOW changes on orbital timescales.

TABLE 4

Glacial/Interglacial Averages – Site U1387

Above MIS 16	Calc/Qtz	Dolo/Qtz	Ill/Qtz	7 Å/Qtz	Qtz
Average Glacial	6.85	0.78	*0.33	*0.29	244.40
Average Interglacial	6.24	0.99	*0.31	*0.31	226.12

MIS 16 and Below	Calc/Qtz	Dolo/Qtz	Ill/Qtz	7 Å/Qtz	Qtz
Average Glacial	5.29	1.08	*0.30	*0.33	*249.45
Average Interglacial	4.65	0.91	*0.31	*0.35	*254.82

Glacial/Interglacial Averages – Site U1389

Above MIS 16	Calc/Qtz	Dolo/Qtz	Ill/Qtz	7 Å/Qtz	Qtz
Average Glacial	4.18	0.78	*0.20	0.32	*328.53
Average Interglacial	4.63	0.90	*0.20	0.29	*322.06

MIS 16 and Below	Calc/Qtz	Dolo/Qtz	Ill/Qtz	7 Å/Qtz	Qtz
Average Glacial	4.30	0.85	*0.21	0.35	306.28
Average Interglacial	4.96	0.99	*0.22	0.41	249.41

*Change between average value in glacial and interglacial periods is within analytical uncertainty

TABLE 5

Mineral Changes Outside Analytical Uncertainty

Above MIS 16	Glacial	Interglacial
Site U1387	↑ Calcite, Quartz ↓ Dolomite	↑ Dolomite ↓ Calcite, Quartz
Site U1389	↑ 7Å ↓ Calcite, Dolomite	↑ Calcite, Dolomite ↓ 7Å

MIS 16 and Below	Glacial	Interglacial
Site U1387	↑ Calcite, Dolomite	↓ Calcite, Dolomite
Site U1389	↑ Quartz ↓ Calcite, Dolomite, 7Å	↑ Calcite, Dolomite, 7Å ↓ Quartz

-Mineral changes within analytical uncertainty are not included in table

-Red denotes MOW core is expected to have been positioned at that site

SUGGESTIONS FOR FUTURE RESEARCH

Since a semiquantitative analysis using mineralogy is not an effective proxy to see MOW changes on orbital timescales, future work with these samples would require additional means of analysis. There are a few approaches that could be attempted. A comparison between data of all students working on the project could reveal patterns over a longer time span. There are currently multiple students working on samples ranging in age from recent to 1.2 Ma.

Another approach would involve adding a measured internal standard before XRD scanning, such as boehmite, corundum, or ZnO. This would allow more quantitative measures of mineral abundances, so that mineral abundances could be compared between different minerals in the same sample, and in samples throughout time.

Since we were unable to differentiate among kaolinite, chlorite, and smectite in this study, another option would be re-analyzing samples using oriented slides and ethylene glycolation. This would determine the specific clays that are present and could be used to see if there are different patterns between the two sites over time.

Determination of grain size changes throughout time at the different sites would allow for a study that is centered more on current velocity, and could help account for some of the other influences that affect the study when looking solely at mineralogy.

Lastly, a study of the same samples using X-Ray Fluorescence (XRF) would allow for a more in-depth study using the ratio of Zr to Al to identify current velocity changes and other elemental assemblages to more clearly distinguish various sediment sources. This was done in a recent study by Bahr et al. (2014).

REFERENCES

Bahr, A., Jimenez-Espejo, F. J., Kolasinac, N., Grunert, P., Hernandez-Molina, F. J., Roehl, U., Voelker, A. H. L., Escutia, C., Stow, D. A. V., Hodell, D., & Alvarez-Zarikian, C. A. (2014). Deciphering bottom current velocity and paleoclimate signals from contourite deposits in the Gulf of Cadiz during the last 140 kyr: An inorganic geochemical approach. *Geochemistry Geophysics Geosystems, 15*(8), 3145-3160.

Baringer, M. O., & Price, J. F. (1999). A review of the physical oceanography of the Mediterranean Outflow. *Marine Geology, 155*(1–2), 63-82.

Brindley, G. W. (1955). Identification of clay minerals by x-ray diffraction analysis, Clays and Clay Minerals, 1, no. 1, 119-129.

Chen, P. (1977). Table of key lines in X-ray powder diffraction patterns of minerals in clays and associated rocks. *Geological Survey Occasional Paper 21,* Indiana Geological Survey, 67 pp.

Gibbons, W., & Moreno, T., (2002). *The geology of Spain*. London: Geological Society.

Hernández-Molina, F. J., Llave, E., & Stow, D. A. V. (2008). Continental slope contourites. *Developments in Sedimentology, 60*, 379-408.

Hernandez-Molina, F., et al., Francisco Javier, Nuno Serra, Dorik A. V. Stow, Estefanía Llave, Gemma Ercilla, and David Van Rooij. (2011). Along-slope oceanographic processes and sedimentary products around the Iberian margin. *Geo-Marine Letters, 31*(5-6), 315-341.

Hernandez-Molina, F., Stow, D. A. V., & Alvarez-Zarikian, C. (2013a). IODP Expedition 339 in the Gulf of Cadiz and off west Iberia; Decoding the Environmental Significance of the Mediterranean Outflow Water and its Global Influence. *Scientific Drilling, 16*, 1-11.

Hernandez-Molina, F., Stow, D.A.V., Zarikian, C., and Shipboard Scientific Party, (2013b). Expedition 339 Summary. *Proceedings of the Integrated Ocean Drilling Program [Online], 339*.

Hernandez-Molina, F. J., E. Llave, B. Preu, G. Ercilla, A. Fontan, M. Bruno, N. Serra, J. J. Gomiz, R. E. Brackenridge, F. J. Sierro, D. A. V. Stow, M. Garcia, C. Juan, N. Sandoval, and A. Arnaiz. (2014a). Contourite processes associated with the Mediterranean Outflow Water after its exit from the Strait of Gibraltar; global and conceptual implications. *Geology 42(3): 227-230*.

Hernandez-Molina, F. J., D. A. V. Stow, C. A. Alvarez-Zarikian, G. Acton, A. Bahr, B. Balestra, E. Ducassou, R. Flood, J.-A. Flores, S. Furota, P. Grunert, D. Hodell, F. Jimenez-Espejo, J. K. Kim, L. Krissek, J. Kuroda, B. Li, E. Llave, J. Lofi, L. Lourens, M. Miller, F. Nanayama, N. Nishida, C. Richter, C. Roque, H. Pereira, M. F. Sanchez Goni, F. J. Sierro, A. D. Singh, C. Sloss, Y. Takashimizu, A. Tzanova, A. Voelker, T. Williams, and C. Xuan. (2014b). Onset of Mediterranean Outflow into the North Atlantic. *Science (New York, N.Y.), 344*(6189), 1244-1250.

Lisiecki, L. E., & Raymo, M. E. (2005a). A Pliocene-Pleistocene stack of 57 globally distributed benthic delta $\delta^{18}O$ records. *Paleoceanography, 20*(1; 1)

Lisiecki, L. E., and M. E. Raymo. (2005b) "LR04 Benthic Stack." LR04 Benthic Stack, Web. <http://www.lorraine-lisiecki.com/LR04_MISboundaries.txt>.

Llave, E., Hernández-Molina, F. J., Ercilla, G., Stow, Dorrik A. V., and Medialdea, T. (2011). Pliocene-Quaternary contourites along the northern Gulf of Cadiz margin: Sedimentary stacking pattern and regional distribution. *Geo-Marine Letters, 31*(5-6), 377-390.

O'Brien, S. (2014). The Gulf of Cadiz Contourite Laboratory: Sediment variability from Recent to 300kya. Unpublished B.S. Thesis, Ohio State University, 30 pp.

Rebesco, M., Hernández-Molina, F. J., Van Rooij, D., & Wåhlin, A. (2014). Contourites and associated sediments controlled by deep-water circulation processes: State-of-the-art and future considerations. *Marine Geology, 352*, 111-154.

Stow, D. A. V., & Faugères, J. (2008). Contourite facies and the facies model. *Developments in Sedimentology, 60*, 223-256.

Stow, D. A. V., Hernandez-Molina, F., Llave, E., Bruno, M., Garcia, M., Diaz, d. R., Somoza, L., & Brackenridge, R. E. (2013). The Cadiz contourite channel; sandy contourites, bedforms and dynamic current interaction. *Marine Geology, 343*, 99-114.

Toucanne, S., Mulder, T., Schoenfeld, J., Hanquiez, V., Gonthier, E., Duprat, J., Cremer, M., & Zaragosi, S. (2007). Contourites of the Gulf of Cadiz; a high-resolution record of the paleocirculation of the Mediterranean Outflow Water during the last 50,000 years. *Palaeogeography, Palaeoclimatology, Palaeoecology, 246*(2-4; 2-4), 354-366.

Viana, A. R. (2008). Economic relevance of contourites. *Developments in Sedimentology, 60*, 491-510.

APPENDIX A

IODP Sample List – Site U1387

Hole	Core	Section	Top Depth	Bottom Depth	MBSF Top	MCD Top	Sample
B	10	1	40	42	84.9	90.72	4538278
B	10	6	105	107	93.05	98.87	4538582
B	11	3	75	77	97.85	104.67	4538681
B	11	4	73	75	99.33	106.15	4538709
A	12	7	14	16	102.85	110.11	4538964
A	13	1	70	72	104.2	111.93	4539326
A	13	4	53	55	108.53	116.26	4539465
A	14	1	102	104	114.12	122.85	4540093
B	13	3	20	22	116.5	125.73	4544160
B	13	5	69	71	119.99	129.22	4554220
B	14	3	67	69	126.57	136.12	4556803
B	14	5	100	102	129.9	139.45	4557061
B	15	2	100	102	134.9	146.18	4557291
B	16	2	54	56	144.04	156.18	4557503
B	16	3	72	74	145.72	157.86	4557535
A	17	4	100	102	147.3	159.03	4557562
A	17	5	7	9	147.87	159.6	4557568
B	18	4	74	76	160.64	173.88	4791165
B	18	6	44	46	163.34	176.58	4791260
A	19	2	122	124	163.62	178.23	4791314
A	19	4	70	72	166.1	180.71	4791337
B	19	3	22	24	169.42	182.28	4791295
B	19	5	110	112	173.3	186.16	4791312
A	20	3	8	10	173.47	186.8	4791346
A	20	5	4	6	176.43	189.76	4791360
B	20	2	46	48	177.76	192.02	4791372
B	20	4	70	72	181	195.26	4791385
A	21	2	22	24	181.82	197.36	4680046
A	21	4	147	149	186.07	201.61	4680092
B	21	2	6	8	186.96	204.17	4680182
B	21	4	147	149	191.37	208.58	4680241
A	22	3	147	149	192.99	212.19	4680287
A	22	4	107	109	194.09	213.29	4680315
B	22	2	145	147	197.85	215.7	4680350

Hole	Core	Section	Top Depth	Bottom Depth	MBSF Top	MCD Top	Sample
B	22	5	130	132	202.2	220.05	4680416
A	23	3	21	23	202.41	221.17	4680449
B	23	1	91	93	205.31	224.26	4680507
B	23	4	49	51	209.39	228.34	4789634
A	24	2	34	36	209.58	231.42	4789780
A	24	5	12	14	213.86	235.7	4789860
B	24	3	29	31	217.29	237.42	4789910
B	24	6	30	32	221.8	241.93	4789990
A	25	2	35	37	220.25	243.26	4790127
A	25	4	23	25	223.13	246.14	4790194
B	25	1	146	148	225.06	248.31	4790226
B	25	4	145	147	229.55	252.8	4790353
A	26	3	34.5	36.5	231.345	255.955	4790475
A	26	4	8.5	10.5	232.585	257.195	4790430
B	26	2	32	34	234.92	258.32	4790541
B	26	4	129	131	238.89	262.29	4790621
A	27	2	46	48	239.56	264.17	4790725
A	27	5	146	148	245.06	269.67	4790702
A	28	1	35	37	247.55	272.16	4790887
A	28	3	36	38	250.56	275.17	4790948

IODP Sample List – Site U1389

Hole	Core	Section	Top Depth	Bottom Depth	MBSF Top	MCD Top	Sample
A	13	6	14	16	109.26	121.69	4538677
C	13	2	14	16	114.2	126.57	4538788
C	13	5	14	16	118.7	131.07	4538865
A	15	2	14	16	122.44	136.07	4539320
A	15	4	14	16	125.44	139.07	4539437
C	14	5	14	16	127.93	142.04	4539507
C	14	7	14	16	130.44	144.55	4539544
A	16	3	14	16	132.45	146.77	4539990
A	16	5	14	16	135.45	149.77	4540056
C	15	7	14	16	140.2	154.7	4540134
A	17	2	14	16	140.81	156.14	4540286
A	17	5	14	16	145.31	160.64	4540360
A	17	6	14	16	146.81	162.14	4540385
A	18	2	14	16	151.14	166.52	4542758
A	18	5	14	16	155.64	171.02	4543015
C	18	3	14	16	156.84	173.99	4554184
C	18	4	14	16	158.34	175.49	4554221
A	19	3	14	16	161.28	177.31	4556688
A	19	6	14	16	165.36	181.39	4556782
C	19	4	14	16	166.88	184.07	4556832
C	19	6	14	16	169.81	187	4556869
A	20	2	14	16	169.54	189.01	4556899
A	20	4	14	16	172.54	192.01	4557108
C	20	6	14	16	179.6	199.24	4557247
A	21	3	14	16	180.15	202.39	4557303
A	21	6	14	16	184.65	206.89	4557346
C	21	5	14	16	187.54	210.03	4557414
C	21	7	14	16	190.54	213.03	4557432
A	22	2	14	16	188.78	214.08	4557455
A	22	3	14	16	190.28	215.58	4557462
C	22	4	14	16	195.39	218.99	4557537
C	22	7	14	16	199.89	223.49	4557557
A	23	3	14	16	200.44	227.98	4557579
A	23	6	14	16	204.94	232.48	4557599
C	24	2	14	16	212.94	235.46	4557628
C	24	5	14	16	217.44	239.96	4557639
C	25	1	14	16	221.04	244.12	4557651

Hole	Core	Section	Top Depth	Bottom Depth	MBSF Top	MCD Top	Sample
C	25	4	14	16	225.54	248.62	4557667
A	25	5	14	16	222.24	249.9	4557707
A	25	7	14	16	225.21	252.87	4557729
A	26	2	14	16	227.84	256.29	4557753
A	26	4	14	16	230.84	259.29	4557774
C	26	3	14	16	233.64	262.43	4557800
C	26	5	14	16	236.64	265.43	4557818
A	27	3	14	16	238.28	268.12	4557834
A	27	6	14	16	242.78	272.62	4557856
C	27	4	14	16	244.14	274.02	4557873
C	27	6	14	16	247.14	277.02	4557884
A	28	5	14	16	251.44	283.64	4557942
C	28	2	14	16	251.34	286.43	4557992
C	28	5	14	16	255.84	290.93	4558361
A	29	3	14	16	258.04	292.16	4558372
A	29	6	14	16	262.54	296.66	4558402
C	29	3	14	16	261.8	297.59	4558436
C	29	6	14	16	266.3	302.09	4558468
A	30	5	14	16	269.68	304.32	4558505
A	30	7	14	16	272.68	307.32	4558520
C	30	3	14	16	272.04	309.12	4558536
C	30	6	14	16	276.54	313.62	4558557
A	31	4	13	15	278.83	315.59	4558569
A	31	6	14	16	281.36	318.12	4558581
C	31	4	14	16	282.13	319.8	4558601
C	31	6	14	16	285.13	322.8	4558617
A	32	3	14	16	286.94	325.6	4558654
A	32	5	14	16	289.94	328.6	4558673
C	32	4	14	16	292.74	331.13	4558709
C	32	6	14	16	295.67	334.06	4558782
A	33	1	13	15	293.53	336.1	4558787
A	33	3	14	16	296.54	339.11	4558801
C	33	4	14	16	301.15	341.74	4558825
C	33	6	14	16	304.15	344.74	4558842
A	34	2	14	16	303.81	348.68	4558854
A	34	6	14	16	309.81	354.68	4558899
C	35	2	14	16	318.14	359.08	4558938
C	35	4	14	16	321.14	362.08	4558967
A	35	4	14	16	316.84	363.97	4558975

Hole	Core	Section	Top Depth	Bottom Depth	MBSF Top	MCD Top	Sample
A	35	6	14	16	319.84	366.97	4558992
A	36	1	14	16	321.94	369.17	4559011

APPENDIX B

Marine Isotope Stage Sample Groupings – Site U1387

MIS	Depth (MCD)	Age (kya)
9	90.72	330.43
10	98.87	360.11
11	104.67	381.24
	106.15	386.63
	110.11	401.05
	111.93	407.68
	116.26	423.45
12	122.85	447.45
	125.73	457.94
	129.22	470.65
13	136.12	495.78
	139.45	507.91
	146.18	532.43
14	no samples	
15	156.18	568.85
	157.86	574.97
	159.03	579.23
	159.60	581.30
16	173.88	633.32
	176.58	643.15
	178.23	649.16
	180.71	658.19
	182.28	663.91
17	186.16	678.04
	186.80	680.37
	189.76	691.15
	192.02	699.39
	195.26	711.19
18	197.36	718.84
	201.61	734.32
	204.17	743.64
	208.58	759.70
19	212.19	772.85
	213.29	776.86
	215.70	785.63

MIS	Depth (MCD)	Age (kya)
20	220.05	801.48
	221.17	805.56
	224.26	816.81
	228.34	831.67
21	231.42	842.89
	235.70	858.48
	237.42	864.74
	241.93	881.17
22	243.26	886.02
	246.14	896.51
23	248.31	904.41
24	252.80	920.76
	255.96	932.25
	257.20	936.77
25	258.32	940.87
	262.29	955.33
26	264.17	962.18
27	269.67	982.21
28	272.16	991.28
	275.17	1002.24

Marine Isotope Stage Sample Groupings – Site U1389

MIS	Depth (MCD)	Age (kya)
9	156.14	300.27
	160.64	308.93
	162.14	311.81
	166.52	320.23
	171.02	328.89
	173.99	334.60
10	175.49	337.48
	177.31	340.98
	181.39	348.83
	184.07	353.98
	187.00	359.62
	189.01	363.48
	192.01	369.25
11	199.24	383.16
	202.39	389.22
	206.89	397.87
	210.03	403.91
	213.03	409.68
	214.08	411.70
	215.58	414.58
	218.99	421.14
12	223.49	429.79
	227.98	438.43
	232.48	447.08
	235.46	452.81
	239.96	466.31
13	244.12	483.68
	248.62	502.48
	249.90	507.82
	252.87	520.23
14	256.29	534.51
	259.29	547.04
	262.43	560.16
15	265.43	572.69
	268.12	583.92
	272.62	602.72
	274.02	608.57
	277.02	621.10

MIS	Depth (MCD)	Age (kya)
16	279.14	629.95
	283.64	648.75
	286.43	660.40
17	290.93	679.19
	292.16	684.33
	296.66	703.13
	297.59	707.01
18	302.09	725.81
	304.32	735.12
	307.32	747.65
	309.12	755.17
19	313.62	773.96
	315.59	782.19
20	318.12	792.76
	319.80	799.77
	322.80	812.30
21	325.60	824.00
	328.60	836.53
	331.13	847.10
	334.06	859.33
22	336.10	867.86
	339.11	880.43
	341.74	891.41
23	344.74	903.94
24	348.68	920.40
25	354.68	945.46
26	359.08	963.84
27	362.08	976.37
28	363.97	984.26
	366.97	996.79
	369.17	1005.98

APPENDIX C

Mineral Peak Areas – Site U1387

Depth (MCD)	Age (kya)	Quartz	Calcite	Dolomite	Illite	7 Å
90.72	330.43	168.78	1188.52	200.79	61.60	71.90
98.87	360.11	210.51	1668.54	194.40	66.00	57.90
104.67	381.24	256.91	2056.94	181.58	77.00	81.60
106.15	386.63	251.13	1775.44	190.35	33.00	54.50
110.11	401.05	205.29	1289.64	228.54	52.00	64.40
111.93	407.68	179.94	1358.63	195.38	103.90	75.20
116.26	423.45	221.68	1279.61	246.09	67.80	66.40
122.85	447.45	409.71	1126.28	310.32	158.20	109.70
125.73	457.94	209.32	1765.26	139.68	79.50	76.30
129.22	470.65	215.86	1327.34	105.89	53.50	62.00
136.12	495.78	336.48	1163.70	325.52	78.10	58.10
139.45	507.91	331.47	1508.10	366.87	84.10	55.10
146.18	532.43	191.85	1200.42	81.84	58.80	53.30
156.18	568.85	254.61	1332.55	293.78	48.50	84.60
157.86	574.97	189.78	1304.41	196.60	64.00	93.50
159.03	579.23	231.46	1006.41	207.63	81.10	64.80
159.60	581.30	248.23	1049.59	249.84	118.20	114.10
173.88	633.32	262.23	1332.09	260.80	84.40	56.70
176.58	643.15	271.75	1106.44	340.60	118.40	96.60
178.23	649.16	240.24	1092.95	139.28	84.40	62.70
180.71	658.19	279.30	1677.69	287.73	56.70	76.00
182.28	663.91	222.03	1195.60	218.50	79.00	59.40
186.16	678.04	246.87	1096.43	252.29	69.00	73.40
186.80	680.37	221.62	1086.51	249.70	59.80	69.90
189.76	691.15	265.84	1226.67	248.25	108.70	123.40
192.02	699.39	263.66	1187.61	446.81	125.00	116.80
195.26	711.19	310.49	1027.84	329.59	105.20	100.90
197.36	718.84	262.64	1281.34	304.32	77.80	95.60
201.61	734.32	196.41	1600.62	189.55	68.60	75.40
204.17	743.64	302.79	1349.59	416.97	113.60	122.40
208.58	759.70	249.69	1300.65	244.86	96.90	100.40
212.19	772.85	227.58	1249.93	245.86	85.70	86.20
213.29	776.86	272.73	1391.71	312.04	73.30	101.80
215.70	785.63	194.12	1393.62	170.10	71.40	113.40
220.05	801.48	208.30	1251.05	262.99	95.10	92.90
221.17	805.56	308.28	1290.07	458.22	97.40	111.60

Depth (MCD)	Age (kya)	Quartz	Calcite	Dolomite	Illite	7 Å
224.26	816.81	260.66	1405.20	279.99	62.90	84.10
228.34	831.67	238.87	1367.17	190.08	80.70	99.60
231.42	842.89	262.32	1054.44	310.05	78.10	104.10
235.70	858.48	284.13	1421.16	441.90	82.00	88.10
237.42	864.74	204.16	1210.45	145.75	52.40	84.20
241.93	881.17	192.27	1312.38	161.70	60.40	56.30
243.26	886.02	220.12	1095.28	273.28	66.40	83.10
246.14	896.51	312.86	1255.75	379.05	57.40	49.50
248.31	904.41	216.54	812.10	129.06	81.70	70.20
252.80	920.76	148.42	1315.51	124.53	43.50	54.90
255.96	932.25	289.53	1553.63	365.08	96.70	115.70
257.20	936.77	343.15	1513.04	358.81	92.80	85.50
258.32	940.87	210.35	1445.30	129.03	47.40	79.40
262.29	955.33	239.45	1098.72	217.35	32.90	71.00
264.17	962.18	258.57	1178.63	319.08	57.00	80.50
269.67	982.21	304.88	1026.40	227.31	90.50	89.90
272.16	991.28	239.33	935.78	144.60	69.90	76.20
275.17	1002.24	281.82	1333.02	244.59	43.80	60.00

Mineral Peak Areas – Site U1389

Depth (MCD)	Age (kya)	Quartz	Calcite	Dolomite	Illite	7 Å
156.14	300.27	339.48	1351.37	229.59	62.40	76.80
160.64	308.93	301.48	1270.91	153.15	47.10	67.50
162.14	311.81	429.15	1337.64	756.75	88.30	109.20
166.52	320.23	258.59	1271.48	327.52	64.00	100.50
171.02	328.89	363.71	1179.18	416.27	117.60	83.80
173.99	334.60	409.07	1118.87	505.57	132.80	122.80
175.49	337.48	411.54	1115.07	604.00	130.30	122.10
177.31	340.98	492.44	1239.79	282.17	72.10	94.70
181.39	348.83	355.67	1378.99	293.13	46.10	69.20
184.07	353.98	272.40	1376.11	192.09	59.90	115.50
187.00	359.62	392.25	1507.68	426.93	51.50	80.70
189.01	363.48	244.90	1398.93	241.81	49.00	107.60
192.01	369.25	238.40	1411.31	159.47	52.20	82.20
199.24	383.16	463.94	1604.59	629.49	64.40	115.80
202.39	389.22	217.38	1600.02	139.39	56.50	108.50
206.89	397.87	317.04	1510.01	269.94	47.90	73.60
210.03	403.91	266.55	1461.64	628.37	52.00	84.00
213.03	409.68	225.01	1371.18	126.17	39.50	62.70
214.08	411.70	208.95	1459.10	349.77	58.40	81.80
215.58	414.58	408.78	1306.23	474.65	36.90	69.00
218.99	421.14	159.24	1268.38	199.24	77.00	99.40
223.49	429.79	258.05	1130.46	254.27	30.20	93.40
227.98	438.43	237.92	1074.86	211.13	65.50	132.30
232.48	447.08	193.15	1390.98	132.90	43.70	72.60
235.46	452.81	435.60	1132.62	432.11	108.80	109.60
239.96	466.31	294.81	1172.65	358.39	94.60	116.30
244.12	483.68	219.72	1460.40	112.41	54.60	92.00
248.62	502.48	501.18	1438.01	192.84	33.70	64.10
249.90	507.82	405.27	1537.28	204.31	47.50	86.20
252.87	520.23	247.09	1397.92	172.38	32.50	95.20
256.29	534.51	310.02	1232.32	97.24	45.80	113.80
259.29	547.04	467.95	1414.35	366.24	68.60	74.90
262.43	560.16	295.23	1280.31	106.50	55.20	89.60
265.43	572.69	282.32	1369.77	158.22	66.20	79.30
268.12	583.92	359.99	1266.76	293.02	47.50	84.30
272.62	602.72	246.05	1475.07	174.66	50.80	71.60
274.02	608.57	354.21	1097.16	340.91	73.40	107.60
277.02	621.10	314.05	1421.97	231.29	66.40	78.70
279.14	629.95	275.02	1256.76	195.21	35.20	85.00

Depth (MCD)	Age (kya)	Quartz	Calcite	Dolomite	Illite	7 Å
283.64	648.75	744.72	1488.33	703.21	57.60	59.00
286.43	660.40	233.95	1269.28	126.68	69.30	116.00
290.93	679.19	175.98	1172.13	112.24	45.90	88.50
292.16	684.33	301.71	1283.46	222.30	40.00	119.90
296.66	703.13	227.55	1365.60	168.93	79.50	83.20
297.59	707.01	216.85	982.32	135.39	63.50	105.10
302.09	725.81	234.39	1178.68	122.40	51.20	126.10
304.32	735.12	215.69	1026.61	250.01	64.90	83.20
307.32	747.65	228.49	972.54	218.88	63.90	85.00
309.12	755.17	207.04	1119.01	306.39	38.80	119.00
313.62	773.96	241.48	1222.07	274.77	34.00	59.50
315.59	782.19	293.44	1266.27	379.28	73.90	105.10
318.12	792.76	294.00	1167.75	309.67	64.70	100.50
319.80	799.77	190.62	1207.89	212.55	51.10	84.10
322.80	812.30	251.48	1127.40	162.54	85.00	99.20
325.60	824.00	232.41	1066.05	193.23	48.20	97.30
328.60	836.53	404.74	1034.91	395.13	86.60	100.40
331.13	847.10	239.94	1121.16	556.79	65.30	106.00
334.06	859.33	248.11	1215.61	291.05	71.90	111.80
336.10	867.86	284.69	1106.87	203.13	52.70	89.40
339.11	880.43	415.23	1081.78	251.29	41.60	75.70
341.74	891.41	210.42	1272.27	155.55	61.20	130.00
344.74	903.94	299.76	1074.62	389.08	36.40	85.50
348.68	920.40	340.33	1155.60	292.94	51.30	90.50
354.68	945.46	219.19	1085.35	145.95	44.00	116.80
359.08	963.84	254.07	1305.85	212.83	70.30	80.20
362.08	976.37	198.23	1391.16	151.39	55.40	105.20
363.97	984.26	322.85	1071.42	94.78	59.70	97.70
366.97	996.79	224.04	1142.50	235.94	46.10	125.80
369.17	1005.98	537.47	1309.23	645.77	66.40	75.40

APPENDIX D

Mineral/Quartz Ratios – Site U1387

Depth (MCD)	Age (kya)	Calc/Qtz	Dolo/Qtz	Ill/Qtz	7 Å/Qtz
90.72	330.43	7.04	1.19	0.36	0.43
98.87	360.11	7.93	0.92	0.31	0.28
104.67	381.24	8.01	0.71	0.30	0.32
106.15	386.63	7.07	0.76	0.13	0.22
110.11	401.05	6.28	1.11	0.25	0.31
111.93	407.68	7.55	1.09	0.58	0.42
116.26	423.45	5.77	1.11	0.31	0.30
122.85	447.45	2.75	0.76	0.39	0.27
125.73	457.94	8.43	0.67	0.38	0.36
129.22	470.65	6.15	0.49	0.25	0.29
136.12	495.78	3.46	0.97	0.23	0.17
139.45	507.91	4.55	1.11	0.25	0.17
146.18	532.43	6.26	0.43	0.31	0.28
156.18	568.85	5.23	1.15	0.19	0.33
157.86	574.97	6.87	1.04	0.34	0.49
159.03	579.23	4.35	0.90	0.35	0.28
159.60	581.30	4.23	1.01	0.48	0.46
173.88	633.32	5.08	0.99	0.32	0.22
176.58	643.15	4.07	1.25	0.44	0.36
178.23	649.16	4.55	0.58	0.35	0.26
180.71	658.19	6.01	1.03	0.20	0.27
182.28	663.91	5.38	0.98	0.36	0.27
186.16	678.04	4.44	1.02	0.28	0.30
186.80	680.37	4.90	1.13	0.27	0.32
189.76	691.15	4.61	0.93	0.41	0.46
192.02	699.39	4.50	1.69	0.47	0.44
195.26	711.19	3.31	1.06	0.34	0.32
197.36	718.84	4.88	1.16	0.30	0.36
201.61	734.32	8.15	0.97	0.35	0.38
204.17	743.64	4.46	1.38	0.38	0.40
208.58	759.70	5.21	0.98	0.39	0.40
212.19	772.85	5.49	1.08	0.38	0.38
213.29	776.86	5.10	1.14	0.27	0.37
215.70	785.63	7.18	0.88	0.37	0.58
220.05	801.48	6.01	1.26	0.46	0.45
221.17	805.56	4.18	1.49	0.32	0.36

Depth (MCD)	Age (kya)	Calc/Qtz	Dolo/Qtz	Ill/Qtz	7 Å/Qtz
224.26	816.81	5.39	1.07	0.24	0.32
228.34	831.67	5.72	0.80	0.34	0.42
231.42	842.89	4.02	1.18	0.30	0.40
235.70	858.48	5.00	1.56	0.29	0.31
237.42	864.74	5.93	0.71	0.26	0.41
241.93	881.17	6.83	0.84	0.31	0.29
243.26	886.02	4.98	1.24	0.30	0.38
246.14	896.51	4.01	1.21	0.18	0.16
248.31	904.41	3.75	0.60	0.38	0.32
252.80	920.76	8.86	0.84	0.29	0.37
255.96	932.25	5.37	1.26	0.33	0.40
257.20	936.77	4.41	1.05	0.27	0.25
258.32	940.87	6.87	0.61	0.23	0.38
262.29	955.33	4.59	0.91	0.14	0.30
264.17	962.18	4.56	1.23	0.22	0.31
269.67	982.21	3.37	0.75	0.30	0.29
272.16	991.28	3.91	0.60	0.29	0.32
275.17	1002.24	4.73	0.87	0.16	0.21

Mineral/Quartz Ratios – Site U1389

Depth (MCD)	Age (kya)	Calc/Qtz	Dolo/Qtz	Ill/Qtz	7 Å/Qtz
156.14	300.27	3.98	0.68	0.18	0.23
160.64	308.93	4.22	0.51	0.16	0.22
162.14	311.81	3.12	1.76	0.21	0.25
166.52	320.23	4.92	1.27	0.25	0.39
171.02	328.89	3.24	1.14	0.32	0.23
173.99	334.60	2.74	1.24	0.32	0.30
175.49	337.48	2.71	1.47	0.32	0.30
177.31	340.98	2.52	0.57	0.15	0.19
181.39	348.83	3.88	0.82	0.13	0.19
184.07	353.98	5.05	0.71	0.22	0.42
187.00	359.62	3.84	1.09	0.13	0.21
189.01	363.48	5.71	0.99	0.20	0.44
192.01	369.25	5.92	0.67	0.22	0.34
199.24	383.16	3.46	1.36	0.14	0.25
202.39	389.22	7.36	0.64	0.26	0.50
206.89	397.87	4.76	0.85	0.15	0.23
210.03	403.91	5.48	2.36	0.20	0.32
213.03	409.68	6.09	0.56	0.18	0.28
214.08	411.70	6.98	1.67	0.28	0.39
215.58	414.58	3.20	1.16	0.09	0.17
218.99	421.14	7.97	1.25	0.48	0.62
223.49	429.79	4.38	0.99	0.12	0.36
227.98	438.43	4.52	0.89	0.28	0.56
232.48	447.08	7.20	0.69	0.23	0.38
235.46	452.81	2.60	0.99	0.25	0.25
239.96	466.31	3.98	1.22	0.32	0.39
244.12	483.68	6.65	0.51	0.25	0.42
248.62	502.48	2.87	0.38	0.07	0.13
249.90	507.82	3.79	0.50	0.12	0.21
252.87	520.23	5.66	0.70	0.13	0.39
256.29	534.51	3.97	0.31	0.15	0.37
259.29	547.04	3.02	0.78	0.15	0.16
262.43	560.16	4.34	0.36	0.19	0.30
265.43	572.69	4.85	0.56	0.23	0.28
268.12	583.92	3.52	0.81	0.13	0.23
272.62	602.72	6.00	0.71	0.21	0.29
274.02	608.57	3.10	0.96	0.21	0.30
277.02	621.10	4.53	0.74	0.21	0.25
279.14	629.95	4.57	0.71	0.13	0.31

Depth (MCD)	Age (kya)	Calc/Qtz	Dolo/Qtz	Ill/Qtz	7 Å/Qtz
283.64	648.75	2.00	0.94	0.08	0.08
286.43	660.40	5.43	0.54	0.30	0.50
290.93	679.19	6.66	0.64	0.26	0.50
292.16	684.33	4.25	0.74	0.13	0.40
296.66	703.13	6.00	0.74	0.35	0.37
297.59	707.01	4.53	0.62	0.29	0.48
302.09	725.81	5.03	0.52	0.22	0.54
304.32	735.12	4.76	1.16	0.30	0.39
307.32	747.65	4.26	0.96	0.28	0.37
309.12	755.17	5.40	1.48	0.19	0.57
313.62	773.96	5.06	1.14	0.14	0.25
315.59	782.19	4.32	1.29	0.25	0.36
318.12	792.76	3.97	1.05	0.22	0.34
319.80	799.77	6.34	1.12	0.27	0.44
322.80	812.30	4.48	0.65	0.34	0.39
325.60	824.00	4.59	0.83	0.21	0.42
328.60	836.53	2.56	0.98	0.21	0.25
331.13	847.10	4.67	2.32	0.27	0.44
334.06	859.33	4.90	1.17	0.29	0.45
336.10	867.86	3.89	0.71	0.19	0.31
339.11	880.43	2.61	0.61	0.10	0.18
341.74	891.41	6.05	0.74	0.29	0.62
344.74	903.94	3.58	1.30	0.12	0.29
348.68	920.40	3.40	0.86	0.15	0.27
354.68	945.46	4.95	0.67	0.20	0.53
359.08	963.84	5.14	0.84	0.28	0.32
362.08	976.37	7.02	0.76	0.28	0.53
363.97	984.26	3.32	0.29	0.18	0.30
366.97	996.79	5.10	1.05	0.21	0.56
369.17	1005.98	2.44	1.20	0.12	0.14

APPENDIX E

X-Ray Diffraction Patterns

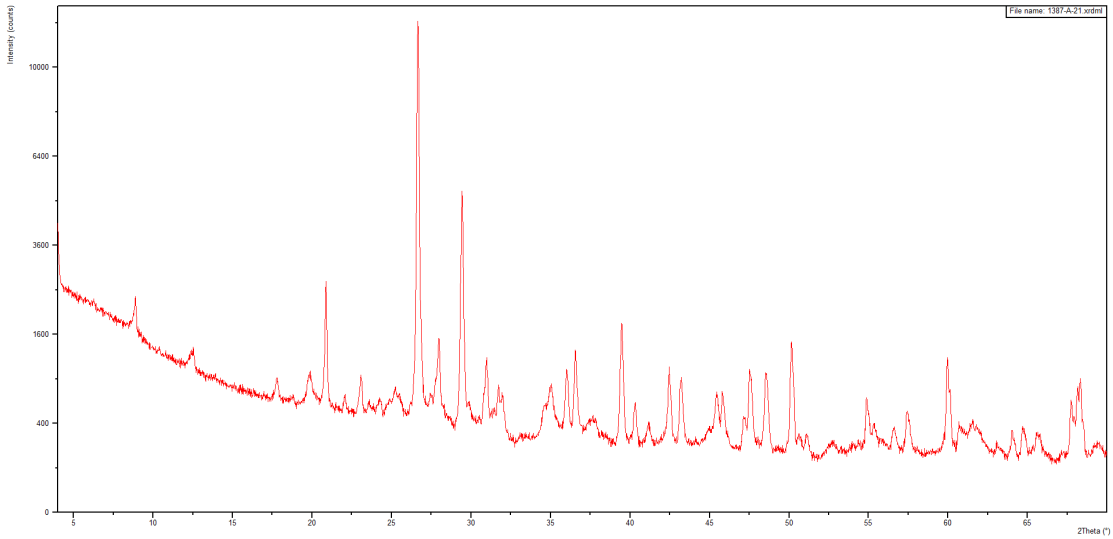

An example of an easy-to-interpret XRD pattern

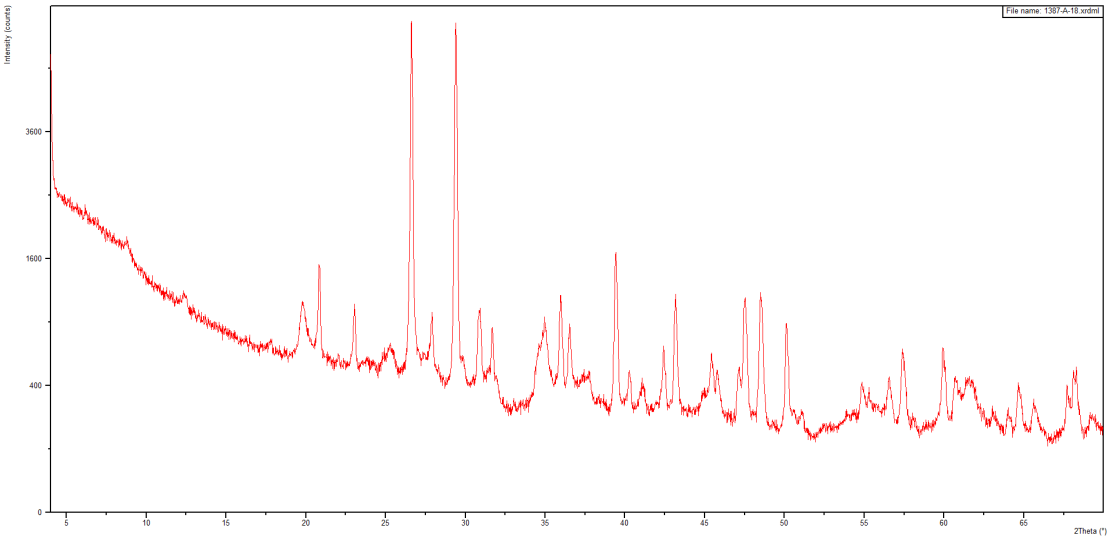

An example of a challenging XRD pattern

APPENDIX F

Standard Operating Procedures – Data Collector (PANalytical Run Parameters)

1.) Open Data Collector Program

2.) File → Open → Browse → [Name Folder] → [Open Last Run File]

3.) Check: Start/End Angle: 4.0-70.0

Step Size: 0.020

Time Per Step: 2.00

→ Comment:

Incident Beam Optics: 1,2

Diffracted Beam Optics: 2,1

T = 27.6

RH = 21%

→ OK

→ Settings:

Tension: 45 kV

Current: 40 mA

4.) Description → [Change to New Sample Name]

5.) File → Save As → [Rename All Samples]

6.) File → Open Program → Measurement Type → Sample Changer Batch → Auto Sample Changer Program → Open

7.) Delete Batches

8.) Insert → Browse → Browse → [Name Folder] → Choose File → Open → OK

*Change Position #

9.) Check X-Ray Settings:

45 kV

20 mA

10.) ☒ → Save

11.) Measure → Program → Sample Changer Batch → Auto Sample Changer Program → Open → OK

Standard Operating Procedures – HighScore (Plus)
(Pattern Analysis)

1.) Open HighScore (Plus)

2.) File → Open → Locate file to analyze (XRDML format)

3.) Treatment → Determine Background

Granularity = 20

Bending Factor = 2

→ Accept

4.) Treatment → Search Peaks

Min. Sig. = 1.00

Min. Tip Width = 0.10

Max. Tip Width = 1.00

Peak Base Width = 2.00

→ Search Peaks → Accept

5.) Treatment → Insert Peak → Zoom in and search for unmarked peaks

*Click on Insert Peak again to turn function off

6.) Analysis → Search & Match → Execute Search & Match

Parameters:

☑ Auto Residue

☑ Match Intensity

☑ Demote Unmatched Strong

Restrictions:

→ Edit Restriction Sets

• Subfiles:

☑ Mineral

• Chemistry:

*Clear All

• Strings:

*Clear All

• Quality:

☑ Skip no RIR Value

→ Close → Search → OK

*Tip: Sometimes the window hides itself. You must bring it back up and click “OK” before you can continue in HighScore (Plus)

7.) Right-click on candidate → Accept candidate

8.) Right-click on Accepted candidate → Analyze Pattern Lines

*Double-click on Accepted candidate or candidate to see card

*Tip: You need to exit card to go back to HighScore (Plus)

*Hover over peak line at top of graph to see d-spacing, then compare to d-spacing of clays from textbook

9.) (Green funnel icon at bottom of screen) Retrieve Pattern by Restrictions, 10-20% of maximum OK

*Last step for leftover peaks